## High gradient tests of metallic mm-wave accelerating structures

Massimo Dal Forno<sup>a</sup>, Valery Dolgashev<sup>a</sup>, Gordon Bowden<sup>a</sup>, Christine Clarke<sup>a</sup>, Mark Hogan<sup>a</sup>, Doug McCormick<sup>a</sup>, Alexander Novokhatski<sup>a</sup>, Brendan O'Shea<sup>a</sup>, Bruno Spataro<sup>b</sup>, Stephen Weathersby<sup>a</sup>, Sami G. Tantawi<sup>a</sup>

<sup>a</sup>SLAC National Accelerator Laboratory, Menlo Park, California 94025, USA <sup>b</sup>INFN/LNF Frascati, Via E. Fermi, 40, Frascati (Roma) 00044, Italy

#### **Abstract**

This paper explores the physics of vacuum rf breakdowns in high gradient mm-wave accelerating structures. We performed a series of experiments with 100 GHz and 200 GHz metallic accelerating structures, at the Facility for Advanced Accelerator Experimental Tests (FACET) at the SLAC National Accelerator Laboratory. This paper presents the experimental results of rf tests of 100 GHz travelling-wave accelerating structures, made of hard copper-silver alloy. The results are compared with pure hard copper structures. The rf fields were excited by the FACET ultra-relativistic electron beam. The accelerating structures have open geometries, 10 cm long, composed of two halves separated by a variable gap. The rf frequency of the fundamental accelerating mode depends on the gap size and can be changed from 90 GHz to 140 GHz. The measured frequency and pulse length are consistent with our simulations. When the beam travels off-axis, a deflecting field is induced in addition to the decelerating longitudinal field. We measured the deflecting forces by observing the displacement of the electron bunch and used this measurement to verify the expected accelerating gradient. We present the first quantitative measurement of rf breakdown rates in 100 GHz copper-silver accelerating structure, which was  $10^{-3}$  per pulse, with peak electric field of 0.42 GV/m, an accelerating gradient of 127 MV/m, at a pulse length of 2.3 ns. The goal of our studies is to understand the physics of gradient limitations in order to increase the energy reach of future accelerators.

#### 1. Introduction

Accelerating gradient is one of the crucial parameters affecting the design, construction and cost of the next generation linear accelerators. The challenge is to develop reliable and cost-effective high-gradient accelerators.

The typical working frequencies of linear accelerators are from about 1 GHz to 12 GHz. The accelerating gradient of the SLAC S-band linac is about 17 MV/m [1]. During development of the Next Linear Collider (NLC)/Global Linear Collider (GLC), an X-band test accelerator operated at 65 MV/m unloaded gradient [2, 3]. The CERN based linear collider design CLIC requires 100 MV/m loaded gradient at 12 GHz in accelerating structures with heavy wakefield damping [4]. Future accelerators like compact synchrotron light sources or inverse Compton scattering gamma ray sources [5] may need even higher gradients.

High gradient acceleration has several problems: rf breakdown, pulsed surface heating and field emission are the major obstacles [6]. RF breakdowns limit the working power and produce irreversible surface damage in high power rf components and rf sources.

#### 1.1. RF breakdown studies

Experimental work on high gradient acceleration was a major part of early linear collider development, published by V. E. Balakin *et. al.* [7] and by G. Loew *et. al.* [8]. The work

directly linked to peak electric field. They were studying the peak limit value of the electric field that generates breakdowns. Their work was carried out at different frequencies: S-band, C-band, and X-band. They found that the maximum peak surface electric field achievable without rf breakdowns, grows with the square-root of the frequency. This analysis lead to the idea that maximum accelerating gradient, limited by breakdown, increases with frequency. Later, other research carried out at CERN [9, 10, 11] in the frequency range from 21 to 39 GHz, concluded that there is no increase in the maximum achievable gradient at higher frequencies. Both studies considered rf breakdown as a phenomenon generated when the peak electric field exceeds a certain threshold.

of G. Loew et. al. [8] considered that the rf breakdowns were

Major studies to understand and mitigate the effects of rf breakdown were conducted during the development of the normal-conducting 11.424 GHz linear collider NLC/GLC [12, 2, 3], which has been followed by the 12 GHz CERN-based linear collider CLIC [13]. During the NLC/GLC work the statistical nature of rf breakdown became apparent [12, 2, 3, 14]. For most accelerating structures exposed to the same rf power and pulse shape, the number of rf breakdowns per pulse is nearly steady or slowly decreasing over  $10^5 - 10^7$  pulses. The breakdown probability became one of the main quantitative requirements characterizing high gradient performance of linacs. For instance: the CLIC linear collider requires rf breakdown probability to be less than  $4 \cdot 10^{-7}$  per pulse per meter for a loaded accelerating gradient of 100 MV/m.

As technology progressed, sophisticated manufacturing and

Email address: dalforno@slac.stanford.edu (Massimo Dal Forno)

surface preparation techniques and systematic rf processing methods were developed [15, 16, 17, 18]. As a result of this R&D, practical 11.4 GHz Traveling Wave (TW) accelerating structures, which are CLIC prototypes, run at breakdown rates of about  $10^{-6}$  per pulse per meter at unloaded gradients up to 120 MV/m and  $\sim$  200 ns pulse length [19]. TW structures that include wakefield damping work at about 100 MV/m for similar breakdown rates [19, 20]. Studies of new geometries and materials at 11.424 GHz show the potential to reach 150 MV/m accelerating gradients with similarly low breakdown rates [21].

Advances in understanding limitations on accelerating gradient go beyond linear colliders. Accelerators are used in applications such as inverse Compton scattering gamma ray sources [5], compact Free-Electron Lasers (FELs) [22, 23], and compact medical linacs for hadron therapy [24]. Modern high gradient devices such as photo-rf guns [25], 4-th harmonic linearizers for FELs [26], rf deflectors [27, 28, 29], and rf undulators [30, 31], all use these technologies and methods, developed and sustained by studies of high gradient accelerators.

Presently, X-band structures are the most studied in terms of rf breakdowns [14, 32, 33, 34, 35]. We know that breakdown statistics depend on pulsed surface heating [36] and a numerous list of other factors, such as the peak electric field, the peak magnetic field [37], and the peak Poynting vector [38]. In our X-band experiments, we found that copper-silver accelerating structures typically have lower breakdown rate than copper structures [14, 9].

In this paper, using all the knowledge and technologies developed in designing, fabricating, and testing for X-band structures, we want to explore the physics of rf breakdowns at sub-THz frequencies.

## 1.2. W-band accelerating structures

W-band metallic and dielectric structures were previously studied at SLAC by Whittum *et. al.* [6, 39, 40, 41, 42, 43, 44]. Also Hill *et. al.* [45, 46, 47, 48] tested both a single metallic W-band cavity and a dielectric linear accelerator excited with an electron beam. They studied the longitudinal and transverse wakefields in a 91 GHz dielectric coated accelerating structure [49]. Henke and Bruns [50, 51, 52, 53] and Chou and Kroll at SLAC designed a W-band muffin-tin planar accelerator structure [54, 55, 56]. These studies highlight the difficulties of working at W-band frequencies. The challenge was to accurately manufacture and assemble the structure from its parts [57].

#### 1.3. Dielectric and metallic wakefield accelerators

Another approach to reaching high accelerating gradients at higher frequencies involves dielectric wakefield accelerators. These schemes have been tested at SLAC FACET [58, 59] and elsewhere [60, 61, 62, 63]. At Argonne, beam driven structures [64, 65, 66, 67], both metallic and dielectric, were also tested. To our knowledge, in these experiments there were no systematic studies of rf breakdown probability.

This paper is divided into five sections. Section 2 reviews the previous experiments and introduces our last experiment: a 100 GHz copper-silver accelerating structure. In the third section we discuss design considerations and the geometry of the structure. In the fourth section we present the rf simulations including the estimation of the pulsed surface heating. The fifth section reports experimental results, comparison with simulations and with previous experiments. Section 6 is the discussion and section 7 the conclusions.

All symbols used in this paper are presented in Table 1.

Table 1: Symbols and abbreviations used in this papers.

	rable 1: Symbols and abbreviations used in this papers.
C	Speed of light
d	Cell length period
$\Delta \phi$	Phase advance
R	Shunt impedance per unit length
$P_d$	Dissipated power in one cell
U	Stored energy in one cell
P	Power flow through the cavity cross-section
$P_{out}$	Total power radiated from the two output horns
$K_Z$	Loss factor per unit length
$v_g$	Group velocity
$ au_F$	Filling time
$ au_D$	Decay time (of the rf power)
$ au_T$	Equivalent pulse length with same peak pulsed heating
$ au_W$	Equivalent pulse length with same pulse energy
$l_{att}$	Attenuation length
V	Integrated accelerating voltage
$E_{acc}$	Accelerating gradient
$E_{max}$	Peak electric field on surface
$H_{max}$	Peak magnetic field on surface
$Q_0$	Unloaded quality factor
$\overline{q}$	Bunch charge
$\sigma_z$	r.m.s. bunch length
L	Length of the accelerating structure
2 <i>a</i>	Gap size between the two halves
e	Electron charge
$\Delta x$	Horizontal beam displacement on the diagnostic screen
$\theta_{x}$	Horizontal kick angle
$V_x$	Deflecting voltage
E	Beam energy
$R_{12}$	Beam optics coefficient that converts a beam horizontal
	angle into a beam horizontal displacement
μ	Magnetic permeability
$\sigma$	Electric conductivity
k	Thermal conductivity
ρ	Copper density
$c_{\epsilon}$	Specific heat

## 2. High gradient mm-wave program at SLAC

As a part of the high gradient research at SLAC, we are studying rf breakdown physics in open metallic accelerating structures at 100 GHz and 200 GHz, made with copper, coppersilver alloy and stainless-steel. The structures were excited by an ultra-relativistic electron beam. The beam was generated by

Experiment No.	Date	Type	Material	Nominal frequency	Bunch charge	r.m.s bunch length
1	Jun 29 - 2012	Standing wave	Cu	100 GHz	2.7 nC	50 μm
2	Mar 28 - 2014	Travelling wave	Cu	100 GHz	3.2 nC	50 μm
3	May 24 - 2014	Travelling wave	S. Steel	100 GHz	3 nC	50 μm
4	Mar 29 - 2015	Travelling wave	Cu	100 GHz	3.2 nC	50 μm
5	Apr 25, 27 - 2015	Travelling wave	Cu	200 GHz	3.2 nC	50 μm
6	May 15 - 2015	Travelling wave	Cu-Ag	200 GHz	1.6 nC	25 μm
7	Nov 21 - 2015	Travelling wave	Cu-Ag	100 GHz	3.2 nC	25 μm
=	Nov 23 - 2015	=	=	=	2.7 nC	25 μm
=	Nov 30 - 2015	=	=	=	2.7 nC	25 μm

Table 2: List of all the mm-wave experiments carried out at FACET.

FACET [58], housed in the first 2 km of the SLAC linear accelerator [1]. The FACET beam energy was 20.35 GeV. The list of all the mm-wave experiments carried out at FACET is in Table 2. All the tested accelerating structures are constant impedance and open, consisting of two separate halves, separated by a gap. In the experiment No. 1 the gap between the two plates was fixed, in the subsequent experiments the gap was varied, changing the rf parameters. The bunch charge was fixed during the experiments, therefore we changed the gradient by varying the relative position of the beam with respect to the center of the structure.

The experiment No. 1 used a travelling wave structure working in the standing wave regime. The coupler is undercoupled with -30 dB of transmission. We found that the useful rf detected signal was low compared to the ambient electromagnetic noise. Thus in all the subsequent experiments we used a travelling wave structure, with a matched coupler with gap =  $0.3 \, \text{mm}$ , to increase the signal to noise ratio. We used travelling wave structures also to compare the performances of mm-wave accelerators with the currently used X-band travelling wave accelerators.

Different materials have been tested, copper (in the Experiments No. 1, 2, 4 and 5), stainless steel (in the Experiment No. 3), and copper-silver (in the Experiments No. 6 and 7). The metals used to produce the structures are not heat treated, we used hard copper (not annealed) and hard copper-silver, because from our X-band experience hard metals have low breakdown rate. We measured the breakdown rate at different nominal frequencies, at 100 GHz (in the Experiments No. 1, 2, 3, 4 and 7) and at 200 GHz (in the Experiments No. 5 and 6). The results of the tests of the 100 GHz structures are presented in the papers [68, 69], while results of the 200 GHz structures tests are presented in [70]. The results of the last, 7th experiment are presented in this paper and compared with the previous ones.

## 2.1. Summary of the first 100 GHz experiments, No. 1, 2 and 3

Results of the first 100 GHz copper and stainless-steel accelerating structures are presented in paper [68]. We found that the non-damage conditions in a 100 GHz copper travelling wave accelerating structure are the following: accelerating gradient of 0.3 GV/m with a peak surface electric field of 1.5 GV/m and a pulse length of about 2.4 ns. In the 100 GHz stainless

steel travelling wave accelerating structure we found an accelerating gradient of 0.19 GV/m with a peak surface electric field of 1 GV/m and a pulse length of about 0.33 ns. In these first experiments we did not measure the breakdown rate. As the studies progressed, we improved our diagnostic tools and introduced the *arc-detector*, a diagnostics unique to open accelerating structures. The two halves are insulated from each other and ground. The *arc-detector* measures the field emission current and reliably detects rf breakdowns. Details of the *arc-detector* are described in the experimental chapter and in ref [68, 70].

## 2.2. Summary of the experiment No. 4, 100 GHz copper structure

The first results of the breakdown rate measurements in 100 GHz copper structures are presented in [69], where we found that the breakdown rate was 0.066 per pulse, with a peak surface electric field of 0.57 GV/m (considering trapped modes synchronous to the electron beam, calculated with a modal expansion method described in [68]), and a pulse length of 2.3 ns. From the wakefield simulations we obtained the electromagnetic fields excited by the bunch which both decelerate and deflect the beam, obtaining the clear relation between deceleration and deflection. In this experiment we measured deflecting voltage by observing the displacement of the electron beam on a diagnostic screen. By knowing the relation between deceleration and deflection, the measurement of the deflecting field allowed us to confirm the simulated values of the deflecting and accelerating gradients.

#### 2.3. Summary of the 200 GHz experiments, No. 5 and 6

Using the experience and techniques developed in our previous 100 GHz tests, we built 200 GHz travelling wave accelerating structures. The first breakdown rate measurements in 200 GHz copper and copper-silver structures are presented in [70]. We found that at 200 GHz the breakdown rate of the copper structure was  $10^{-2}$  per pulse, with a peak surface electric field of 500 MV/m and a rf pulse length of 0.3 ns. In this case the ratio between beam aperture and wavelength was high,  $a/\lambda = 0.5$ , therefore the ratio between peak field and accelerating gradient was 1arge,  $E_{max}/E_{acc} = 8.9$ . Thus the accelerating gradient was 56 MV/m. Typically a high value of  $a/\lambda$  leads to a high value of  $a/\lambda$  leads

 $E_{max}/E_{acc} \sim 2$  with  $a/\lambda = 0.1 \sim 0.2$  [32]. The pulse repetition rate with copper was 1, 9 and 15 Hz. Copper-silver structure had a breakdown rate of  $10^{-2}$  per pulse, with peak electric field of 320 MV/m at a pulse length of 0.5 ns. With  $a/\lambda = 0.37$ ,  $E_{max}/E_{acc} = 6.4$ , this corresponds to an accelerating gradient of 50 MV/m (the repetition rate was 29 Hz).

In the 200 GHz experiments, the breakdown rate was higher in the copper-silver structure, in contradiction with the X-band experiments, where the breakdown rate was higher in copper structures. We speculate that with the copper-silver structure the higher beam repetition rate could have increased the breakdown rate.

## 2.4. Experiment No. 7, 100 GHz copper-silver structure

In this paper we present the results of our last test, Experiment No. 7. We performed quantitative measurements of rf breakdown rates and gradients in a 100 GHz coppersilver structure, and we show the comparison with the previous 100 GHz copper tests No. 1, 2 and 4. We compare the performances of different materials, copper and copper-silver. Motivation to perform 100 GHz test with copper silver was a need to better understand rf performance of this material.

In our X-band experience copper-silver accelerating structures have typically lower breakdown rate than copper structures, and in the 200 GHz experiments, the copper-silver structure performed worse than the copper one, speculated to be due to different experimental conditions. Since the experimental conditions of the 100 GHz experiments No. 4 and 7 are similar, we expect to have a better comparison between copper and copper-silver in the these two tests.

## 3. Design and geometry of the structures

In experiment No. 7, we studied breakdowns in a beam-driven 100 GHz copper-silver structure. The copper-silver alloy contains 0.085% silver. Since we do not have access to mm-wave rf sources, we designed wakefield-excited structures.

We designed the accelerating structures to be constant impedance, open type, composed of two separate movable metal halves. The horizontal position, the vertical position and the gap are remotely controlled by three actuators. The cavities and couplers are milled into the flat side of metal blocks. All the edges have been rounded to minimize the peak fields. When the two halves are placed together, they form a single accelerating structure. The regular cell has been designed with a fundamental mode close to  $2\pi/3$  phase advance, when the gap is set to 0.3 mm. The gap 2a=0.3 mm was chosen to accommodate the practical transverse bunch size.

The rf parameters of the structure can be changed by varying the gap. The whole structure is 10 cm long, with the active length of the accelerating cavities of 8.96 cm. There are 110 regular cavities and two couplers with a matching cells each. Both input and output couplers are symmetric dual-feeds, radiating energy out through antenna horns towards pyrodetectors.

Fig. 1(a) shows a solid model of the output section of the 100 GHz travelling wave accelerating structure. Fig. 1(b) shows

a picture of the output section of the copper-silver structure. When the gap is closed there is no opening for the beam to

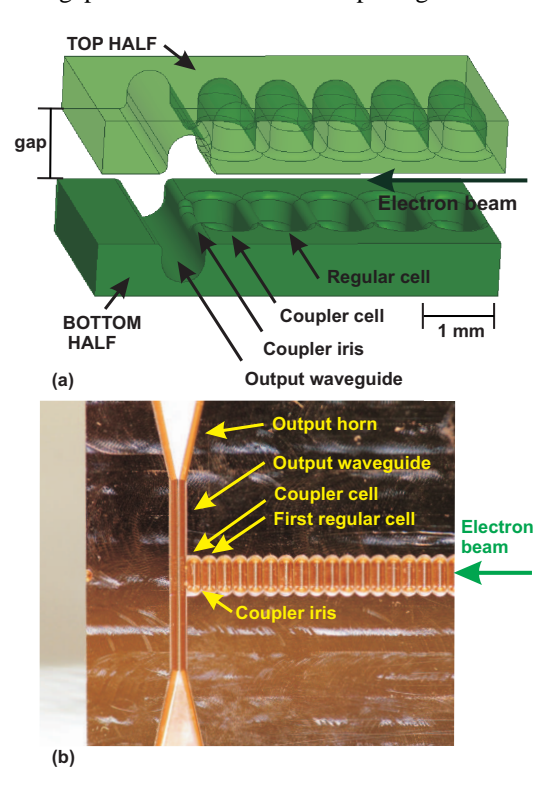


Figure 1: Solid model of the output section of the 100 GHz travelling wave accelerating structure (a), and picture of the output section of the copper-silver structure (b).

travel.

The geometry of the vacuum part of the regular cell and of the coupler is shown in Fig. 4 of paper [68].

## 4. RF simulations

In our experiments the electromagnetic fields in the structure are excited by the FACET ultra-relativistic electron beam. To characterize the beam-structure interaction we simulated the periodic accelerating structure by using one regular cell. We calculate the rf parameters, accelerating gradients and peak fields by using the rf simulation code Ansys HFSS [71]. We used a modal expansion method, described in [68]. We repeat for clarity the relations used to obtain the rf quantities that characterize the structure.

The shunt impedance per unit length is:

$$R = \frac{V^2}{P_d} \frac{1}{d}.\tag{1}$$

The loss factor (per unit length) including the group velocity related compression factor [72, 73, 74] is:

$$\kappa_z = \frac{V^2}{4U} \frac{1}{d} \frac{1}{1 - v_g/c}.$$
 (2)

The group velocity is:

$$v_g = P \cdot d/U. \tag{3}$$

The decay time (of the rf power) is:

$$\tau_D = \frac{Q_0}{\omega_0} \left( 1 - \frac{v_g}{c} \right). \tag{4}$$

The filling time is:

$$\tau_F = \frac{L}{v_g} \left( 1 - \frac{v_g}{c} \right). \tag{5}$$

The attenuation length is:

$$l_{att} = \frac{P}{P_d} d\left(1 - \frac{v_g}{c}\right) = v_g \tau_D. \tag{6}$$

After calculating the above rf parameters, the following expressions are the quantities induced by the beam, for a given mode:

The induced accelerating gradient is:

$$E_{acc} = 2\kappa_z q \, \exp\left(-\frac{\omega_0^2 \sigma_z^2}{2c^2}\right). \tag{7}$$

The induced power flow is:

$$P = \kappa_z q^2 v_g \frac{1}{1 - v_g/c} \exp\left(-\frac{\omega_0^2 \sigma_z^2}{c^2}\right). \tag{8}$$

The pulse energy is:

$$W = \int_{0}^{\tau_F} P \exp\left(-\frac{t}{\tau_D}\right) dt = P \tau_D \left[1 - \exp\left(-\frac{\tau_F}{\tau_D}\right)\right]. \tag{9}$$

#### 4.1. Coupler matching

Practically, the rf coupler can only be matched for a specific gap size. We choose to match the coupler at 0.3 mm gap size and calculate the reflectivity for other gap values. The matching procedure is described in [75, 76]. In these simulations we varied the gap from 0.2 mm to 8 mm. Fig. 2 shows the reflection and power transmission of the coupler for different gap sizes. This plot is an extension of Fig. 10 of paper [68], since in the new copper-silver experiments we explored a new parameter space at large gaps, performing measurements by opening the structure gap up to 7.5 mm.

#### 4.2. Electrical parameters of the 100 GHz accelerating structure

In the following we present the results of the rf simulations for the 100 GHz copper and copper-silver travelling wave accelerating structure.

The rf parameters of the fundamental accelerating mode are listed in Table 3. This is the extension of Table I of paper [69], since in the new copper-silver experiments we explored a new parameter space at large gaps, performing measurements by opening the structure gap up to 7.5 mm. The quality factor  $Q_0$  for copper-silver was calculated by using the copper resistivity. From our X-band experiments the copper-silver structure has practically the same  $Q_0$  as the copper one.

The plot of the group velocity, electric field (accelerating and peak on surface), power and pulse energy of the fundamental

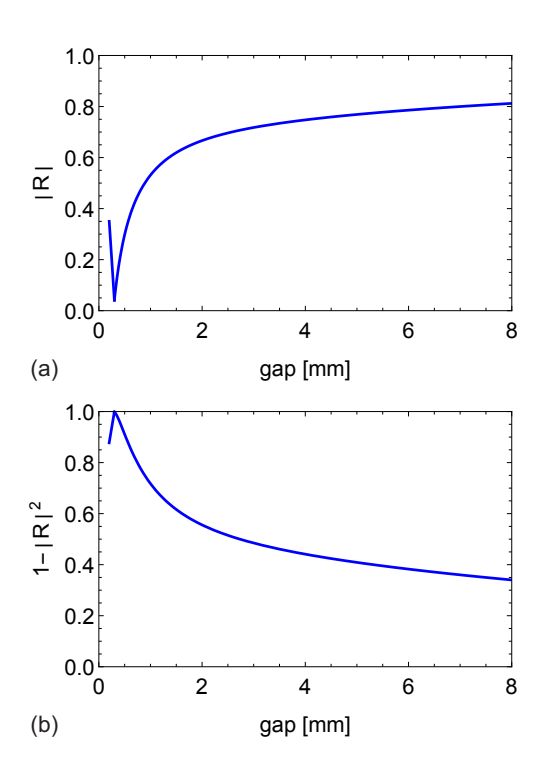


Figure 2: Coupler reflection (a) and power transmission (b) as a function of the gap aperture. The coupler is matched with 0.3 mm gap.

mode are shown in Fig. 3 as a function of the gap size (assuming the beam in the central axis), with 1 nC of bunch charge and  $\sigma_z = 25 \,\mu m$ . The group velocity plots is an extension of Fig. 13 of paper [68], since in the new copper-silver experiments we explored larger gaps, performing measurements by opening the structure gap up to 7.5 mm. The plot of the simulated synchronous frequencies is shown in Fig. 15 of the experimental section, compared with the frequency measurements.

#### 4.3. Radiated power through the output waveguide

With a gap size of 0.3 mm all the rf power is coupled to the output waveguide. For the other gaps the power of the fundamental accelerating mode radiated from the waveguides is calculated by taking into account the reflection as:  $P_{out} = P(1 - |R|^2)$  (the reflection of upstream coupler is ignored). The rf power pulses generated by the 1 nC bunch, with  $\sigma_z = 25 \,\mu m$ , are depicted in Fig. 4, without the coupler reflection (a) and with the coupler reflection (b). The rf output power per each horn is  $P_{out}/2$ , due to the symmetric dual feed coupler type.

#### 4.4. Pulsed surface heating

Cyclic thermal stress produced by rf pulsed heating was identified as a limiting factor for linear accelerators at extremely high frequencies [77, 78, 79]. Pulsed surface heating limited the performance of accelerator couplers at X-band linear accelerators considered for the next linear collider (NLC) [12, 2, 3, 14]. Recent studies of breakdown rates in high gradient linear accelerators showed a direct correlation between these rates and pulsed heating [80].

The correlation of peak pulsed surface heating with rf breakdowns motivated us to evaluate the pulsed surface heating in the

gap	f	$\Delta \phi$	$Q_0$	R	$\kappa_z$	$v_g/c$	$l_{att}$	$\boldsymbol{P}$	$E_{acc}$	$E_{max}$	$H_{max}$
[mm]	[GHz]	[deg]		$[M\Omega/m]$	[MV/(nC m)]	[%]	[mm]	[MW]	[MV/m]	[GV/m]	[MA/m]
0.3	136.27	130.81	2054	398	41.6	0.85	6.08145	0.108	84	0.200	0.364
0.5	130.30	125.20	2021	298	31.15	3.54	25.4071	0.347	63	0.175	0.336
0.7	126.01	121.07	2022	222	23.5	7.65	54.1256	0.588	47	0.155	0.301
0.9	122.66	117.88	2046	166	17.87	12.42	86.8502	0.768	36	0.139	0.269
1.1	119.93	115.24	2089	128	13.89	17.48	119.878	0.890	28	0.127	0.250
1.3	117.59	113.04	2145	99	10.97	22.44	151.625	0.956	22	0.116	0.229
1.5	115.70	111.12	2211	78.2	8.83	27.29	180.984	0.991	18	0.107	0.209
1.7	113.90	109.43	2286	62.5	7.18	31.85	207.87	1.003	14	0.099	0.195
1.9	112.34	107.92	2367	50.7	5.92	36.15	232.068	1.002	12	0.091	0.179
2	111.60	107.24	2411	45.9	5.40	38.18	243.222	0.997	11	0.088	0.169
4	102.30	98.31	3518	10.3	1.38	65.91	368.595	0.797	2.75	0.048	0.098
6	97.46	93.63	4870	3.92	0.58	78.8	398.211	0.647	1.16	0.032	0.067
7.5	95.00	91.25	5969	2.27	0.36	84.2	398.76	0.573	0.72	0.025	0.055

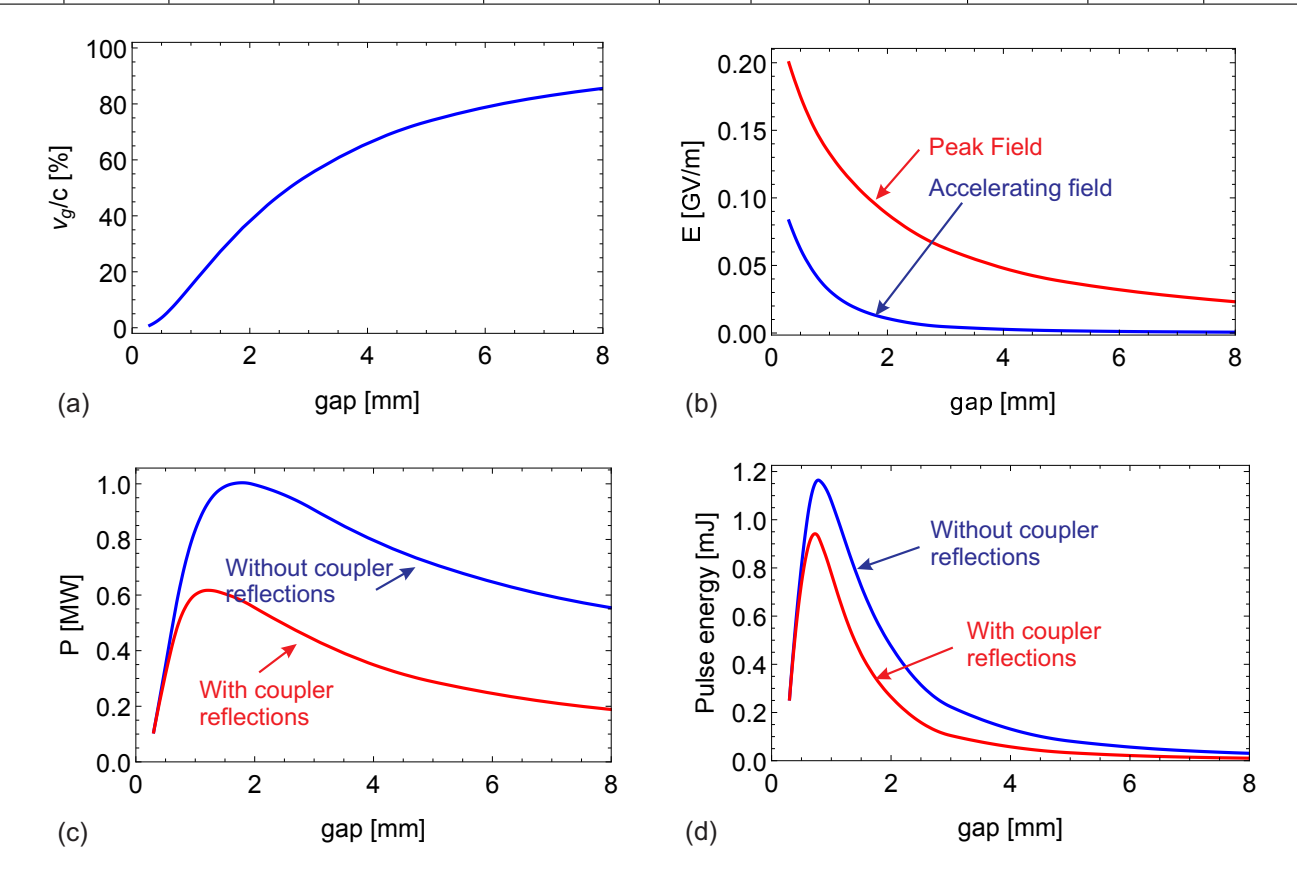


Figure 3: Plot of shunt group velocity (a), accelerating and peak electric field of the fundamental mode (without considering the coupler reflections) (b), maximum power travelling along the cells (max of Fig. 4) and power exiting from the waveguides considering the coupler reflection (c), pulse energy with and without considering the coupler reflection (d). The fields are calculated for an electron beam placed in the central axis. By opening the gap the field is reduced because the interaction decays. The bunch charge is 1 nC and  $\sigma_z = 25 \ \mu m$ .

beam-excited 100 GHz accelerating structures. We analyzed the pulsed heating in a regular cell located near the output coupler by using the following assumptions. We consider fields of only the fundamental mode, without taking into account coupler reflections, therefore we did not consider the increase of pulsed heating due to standing waves caused by coupler reflections. We assumed that there was no increase of conductivity

due to surface roughness and that the metal physical properties did not change during the rf pulse. In the calculations of pulsed heating for copper-silver we used the properties of copper, since a small percentage of silver in the copper does not significantly change the material properties.

The time dependent pulsed surface heating is calculated by

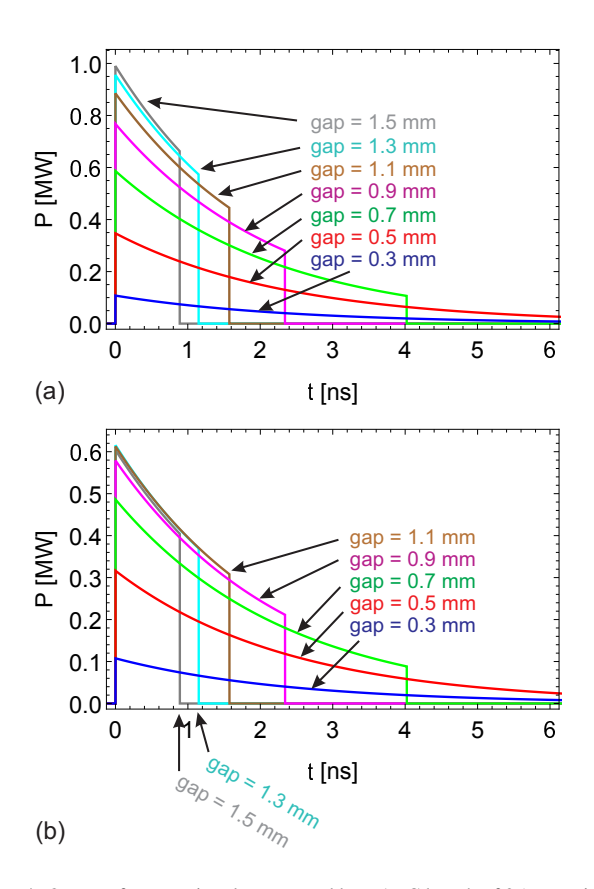


Figure 4: Output rf power signals generated by a 1 nC bunch of  $25~\mu m$ , without coupler reflections (a) and taking into account the coupler reflection as:  $P_{out} = P(1-|R|^2)$ , here the reflection of upstream coupler is ignored (b). The pulse rf durations depends on the group velocity, structure length and attenuation.

using [36, 79]:

$$\Delta T(t) = \frac{1}{2} \sqrt{\frac{f \mu}{k \sigma \rho c_{\epsilon}}} \int_{0}^{t} \frac{H(t')^{2}}{\sqrt{t - t'}} dt', \tag{10}$$

where H(t) is the time-dependent peak surface magnetic field, f is the working frequency,  $\mu$  is the magnetic permeability of copper,  $\sigma$  is the electric conductivity of copper, k is the thermal conductivity of copper,  $\rho$  is the copper-silver allow density supposed to be the same as copper, and  $c_{\epsilon}$  is the specific heat of copper. For a square rf pulse, with amplitude  $H(t) = H_{max}$  and pulse length  $\tau$ , the peak pulsed heating is given by:

$$\Delta T = \sqrt{\frac{f \,\mu}{k \,\sigma \,\rho \,c_{\epsilon}}} |H_{max}|^2 \,\sqrt{\tau}. \tag{11}$$

In our experiments, the pulse of the fundamental mode near the output coupler decays exponentially, and is truncated by the filling time  $\tau_F$  (see Fig. 4). Thus the behavior of H(t) can be modeled as:

$$H(t) = \begin{cases} 0 & \text{if } t < 0, \\ H_{max} e^{-t/(2\tau_D)} & \text{if } 0 < t < \tau_F, \\ 0 & \text{if } t > \tau_F, \end{cases}$$
(12)

which can be integrated analytically.

The calculations of the peak pulsed surface heating in a cell, generated by a 2.7 nC bunch with  $\sigma_z = 25 \ \mu m$ , without taking

into account the coupler reflections are shown in Fig. 5(a), for different gaps. Fig. 5(b) shows the surface peak magnetic field

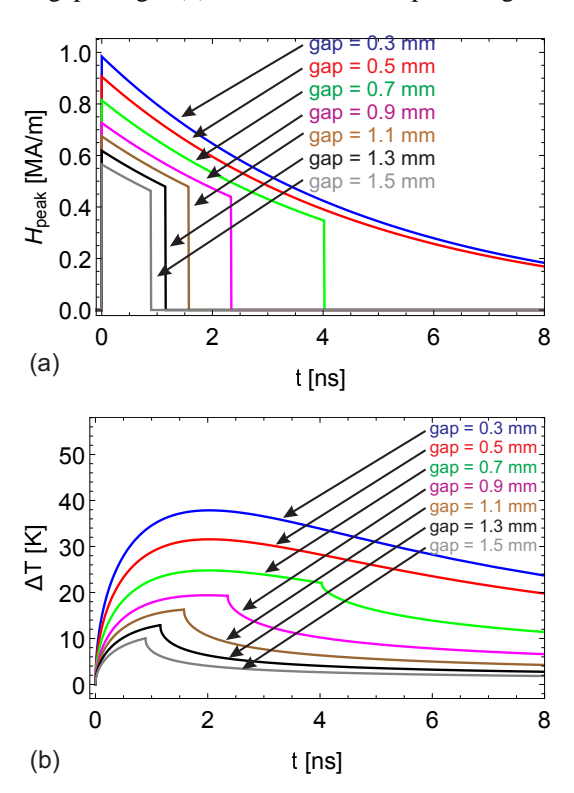


Figure 5: Peak surface magnetic field used to calculate the maximum pulsed surface heating (a). Maximum pulsed surface heating as a function of the time. The coupler reflections are not taken into account (b). The fields of the fundamental mode are generated by 2.7 nC bunch of 25  $\mu m$ .

as a function of time, for the pulse shapes shown in Fig. 4(a).

#### 4.5. RF pulse length

To calculate the pulse length we considered the fields of the fundamental accelerating mode, near the output (downstream) waveguide. As the fundamental mode propagates towards the output waveguide its energy decays due to losses in the metal. Therefore the rf power at the output waveguide is decaying with time constant equal to  $\tau_D$ , and it is truncated with the so-called "filling time", equal to  $\tau_F$ . During the experiment we varied the rf parameters of the structure by remotely changing the gap. With small gaps the losses in the metal are dominant, and therefore the pulse length is equal to the decay time  $\tau_D$ , on the other hand with large gaps the pulse length is determined by the filling time  $\tau_F$ . The plot of the simulated pulse length is shown in Fig. 17 of the experimental section, compared with the pulse length measurements.

In X-band structures there is a strong dependence of the breakdown rate on pulse length [14, 32]. In beam excited structures, the pulse is decaying. Therefore it is hard to compare the results with previous data obtained with structures excited by rf sources, such as klystrons. In order to compare our results with results of structures excited by rf sources we introduced two quantities related to pulse length. We define equivalent rectangular pulse length quantities in order to compare our

beam-excited pulse shapes with simplified rectangular rf pulses. We defined  $\tau_T$  as: the equivalent pulse length which produces the same surface heating as a rectangular one, and  $\tau_W$  as: the equivalent pulse length with the same pulse energy. We refer to Fig. 7 of paper [70], to show the derivations of the equivalent pulse lengths.

We show in Table 4 the pulsed surface heating and equivalent pulse lengths for the 100 GHz copper experiment, with 3.2 nC of bunch charge and  $\sigma_z = 50~\mu m$ , and for the 100 GHz coppersilver experiment, with 2.7 nC of bunch charge and  $\sigma_z = 25~\mu m$ .

#### 4.6. Surface wave

Typically the beampipe of accelerating structures is well below cut-off, for example at X-band  $a/\lambda$  is around  $0.1 \sim 0.2$ , where a is radius of the beampipe [32].

In our open accelerating structure we calculated the rf parameters for different gaps starting from 0.2 mm. We observed that when we opened the gap more than half wavelength, the fundamental accelerating mode is above cut-off, but it remains trapped. Fig. 6 shows the simulation of the synchronous wave in one period of the accelerating structure: gap = 0.5 mm,  $a/\lambda$  = 0.108 (f = 130 GHz) (a); gap = 1.3 mm,  $a/\lambda$  = 0.26 (f = 118 GHz) (b); gap = 4 mm,  $a/\lambda$  = 0.7 (f = 102 GHz) (c); in all three cases the mode is trapped. Thus when the gap is larger than 1.3 mm, the mode is above the beampipe cut-off, but the rf power is guided by the corrugations with no radiation. This behavior is consistent with the so called "surface wave".

Surface waves were studied for applications to communications by [81], showing that guided waves do not necessarily need to be confined within physical boundaries. G.Goubau [82, 83, 84] presented single conductor surface wave transmission lines. W. Rotman studied a single surface corrugated waveguide [85]. A review of surface waves is presented by G. John [86]. H. M. Barlow [87] discussed the different forms of surface waves, behavior and applications. This effect was also studied by Smith-Purcell [88] and used to make high power THz sources [89].

The surface wave is trapped between the structures halves with oversized gaps, it has no radiation losses, while it has wall losses. The electrical parameters presented in Fig. 3 describes the surface wave when the gap is larger than 1.3 mm (when the rf is above cut-off).

We dedicated two shifts for the study of surface waves, on November 21 and November 30, 2015. The results are presented in the experimental section of this paper.

Possible application of surface wave can be beam manipulation, such as beam dechirpers [90, 91], or beam diagnostics such as passive deflectors [92, 93]. The deflecting wakefields create a chirp of deflecting forces over the length of the bunch, which could be used for bunch diagnostics at sub-fs resolution [94, 92, 95]. An algorithm for reconstructing the phasespace of an electron bunch by using a passive deflector is described in [92].

#### 5. Experimental setup and results

In this section we show the experimental results obtained with the 100 GHz copper-silver accelerating structure (Experiment No. 7 of Table 2). Since in our X-band experiments, copper-silver accelerating structures typically have lower breakdown rate than copper structures, we will compare the results of these experiments, with the ones performed with the 100 GHz copper accelerating structure of March 29, 2015 [69] (Experiment No. 4 of Table 2), and with the 200 GHz experiments [70] (Experiments No. 5-6 of Table 2).

## 5.1. Installation of the accelerating structures

The structures were manufactured by the company EDM Department Inc. [96], with precision milling, and cleaned according to SLAC procedure developed for the high-gradient X-band program [97, 98]. The structures, and the remote controlled stages used to align the structures to the beam, were housed in a vacuum chamber in the FACET experimental area, shown in Fig. 7.

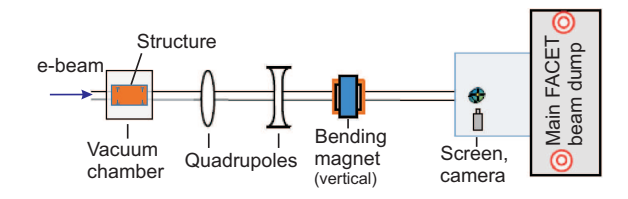


Figure 7: Schematic of the experimental FACET section.

We assembled the two halves of the accelerating structure on remotely controlled motorized stages. Motorized stages are used to shift the structure horizontally (X) or vertically (Y) with respect to the electron beam. There was also a motor to adjust the gap between the two halves of the structure, shown in Fig. 8(b). A mirror is glued to the structure for laser alignment, and a phosphor screen is bolted to the edge of the structure to image the electron beam. The assembly is then installed in the experimental vacuum chamber. The structure antenna horns are directed towards pyrodetectors that sense the pulse energy and towards an interferometer that measures the frequency spectrum of the emitted radiation.

The structure was aligned to the electron beam trajectory by using two methods: with a laser (i) and with a dial gauge with gooseneck (ii). The misalignments called "yaw", "pitch" and "roll" are shown in Fig. 9 and must be reduced.

- (i) Auto collimation to the laser: we used a laser beam aligned to the trajectory of the FACET electron beam during the previous run, as reference. We moved the structure until the laser beam hits the mirror attached to the structure (see Fig. 8(b)) and gets back reflected. We started the alignment procedure by tilting the structure with pitch and yaw adjusting screws. When the back reflected laser beam travels back along the same trajectory as the forward laser beam, the misalignment angles identified as "yaw" and "pitch" (see Fig. 9), are reduced.
- (ii) Roll alignment parallel to the X stage motion (see Fig. 10). For the 100 GHz copper-silver experiment we devel-

Gap No.	gap	f	I	$E_{acc}$	E	max	Н	max	Puls	ed heating	$ au_D$	$ au_F$	$ au_T$	$ au_W$
of Fig. 13	[mm]	[GHz]	[M	V/m]	[G	V/m]	[M.	A/m]		[K]	[ns]	[ns]	[ns]	[ns]
			Cu	CuAg	Cu	CuAg	Cu	CuAg	Cu	CuAg				
1	0.5	130	198	168	0.56	0.47	1.06	0.90	43	31	2.38	9.09	0.70	2.33
2	0.6	128	171	146	0.52	0.44	1.01	0.86	39	28	2.37	6.13	0.69	2.19
3	0.7	126	149	127	0.49	0.42	0.96	0.82	35	25	2.36	4.03	0.69	1.93
4	0.9	123	113	96	0.44	0.38	0.87	0.74	28	20	2.33	2.35	0.68	1.48
5	1	121	100	85	0.42	0.36	0.83	0.70	25	18	2.31	1.92	0.67	1.30
6	1.1	120	88	75	0.40	0.34	0.79	0.67	22	16	2.29	1.57	0.66	1.14
7	1.3	118	70	59	0.37	0.31	0.72	0.61	18	13	2.25	1.15	0.60	0.90
8	1.5	116	56	48	0.34	0.29	0.66	0.56	14	10	2.21	0.89	0.53	0.73
9	2	112	34	29	0.28	0.24	0.55	0.47	8	6	2.13	0.54	0.39	0.48
10	3	106	15	13	0.20	0.17	0.40	0.34	3	2	2.00	0.20	0.18	0.20

Table 4: Electric and magnetic fields, peak pulsed surface heating and equivalent pulse lengths, calculated with the bunch charge and bunch length of the corresponding experiments. The data of the copper experiment (Mar 29, 2015) is with 3.2 nC of bunch charge and  $\sigma_z = 50 \, \mu m$ . The data of the copper-silver experiment, in which we performed the breakdown rate measurements (Nov 23, 2015) is with 2.7 nC of bunch charge and  $\sigma_z = 25 \, \mu m$ .

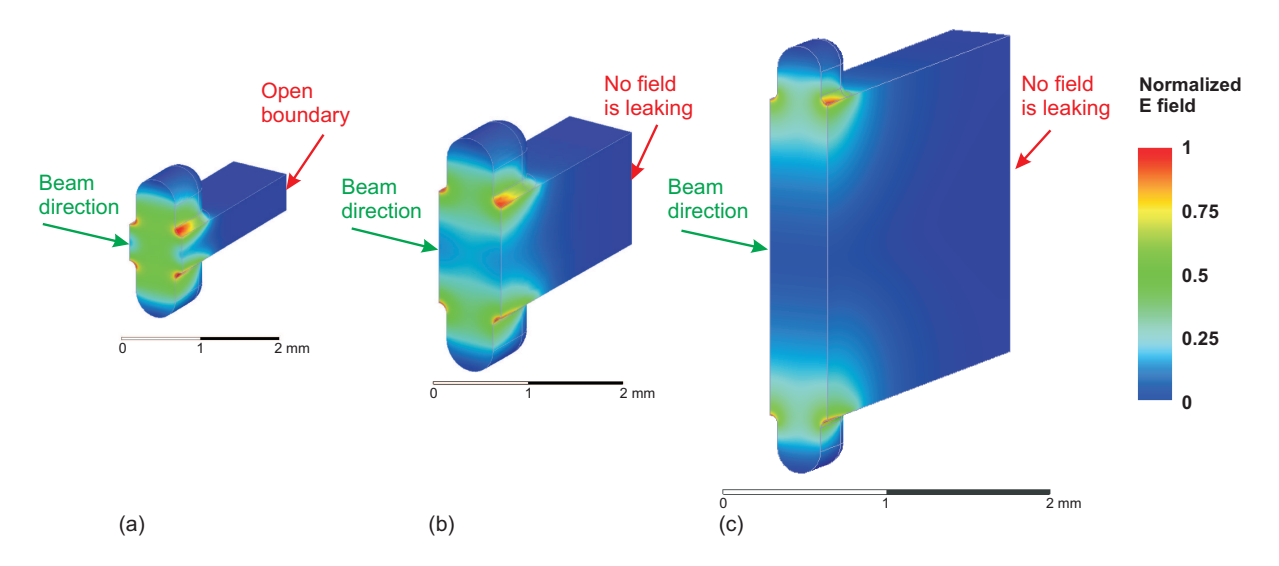


Figure 6: Simulation of the synchronous wave in one period of the accelerating structure (half accelerating structure is shown): gap = 0.5 mm,  $a/\lambda = 0.108$  (f = 130 GHz) (a); gap = 1.3 mm,  $a/\lambda = 0.26$  (f = 118 GHz) (b); gap = 4 mm,  $a/\lambda = 0.7$  (f = 102 GHz) (c); in all three cases the mode is trapped.

oped an additional alignment procedure to reduce the misalignment angle called "roll" (see Fig. 9). A dial gauge, mounted on a gooseneck support touches the top of the structure (see Fig. 10). While moving the structure horizontally in X we observed the displacement on the dial gauge. Roll screws are adjusted to remove any variation of the dial gauge readings. The structure roll is aligned when the gauge reading is practically constant as the structure is moved horizontally. This alignment allows the electron beam to pass cleanly through the gap between the top and bottom halves of the structure.

The two forward output horns radiate the rf power, which is detected by the interferometers and pyro-detectors. For each experiment we recorded the pyrodetector voltage, which is proportional to the pulse energy emitted from the output waveguide horn. The interferometer measures the frequency spectrum of the emitted radiation.

We invented a new diagnostic tool able to reliably detect breakdowns [68]. Since breakdowns generate electron and ion currents, we incorporated an *arc-detector* unique to open structures. The two metal halves that compose the structure were electrically insulated from ground and each other using plastic film. We measured the field emission current and the breakdown current by measuring the voltage induced in the two separate metal blocks. This was achieved by connecting the two metal halves to an oscilloscope (see Fig. 8(c)). A signature of a rf breakdown is a spike in the current monitor signal. We can clearly see voltage spikes of both polarities correlated with the transverse position of the electron beam inside the cavity and the magnitude of the pyrodetector signal. We assumed that these voltage spikes are due to currents generated by rf breakdowns.

The raw signal generated by the pyrodetectors and by the *arc-detector* are processed by a boxcar integrator. A boxcar integrator (other names are gated integrator and boxcar averager) integrates the signal input voltage after a defined waiting time (trigger delay) over a specified period of time (gate width).

After the installation, the vacuum chamber is closed and evacuated.

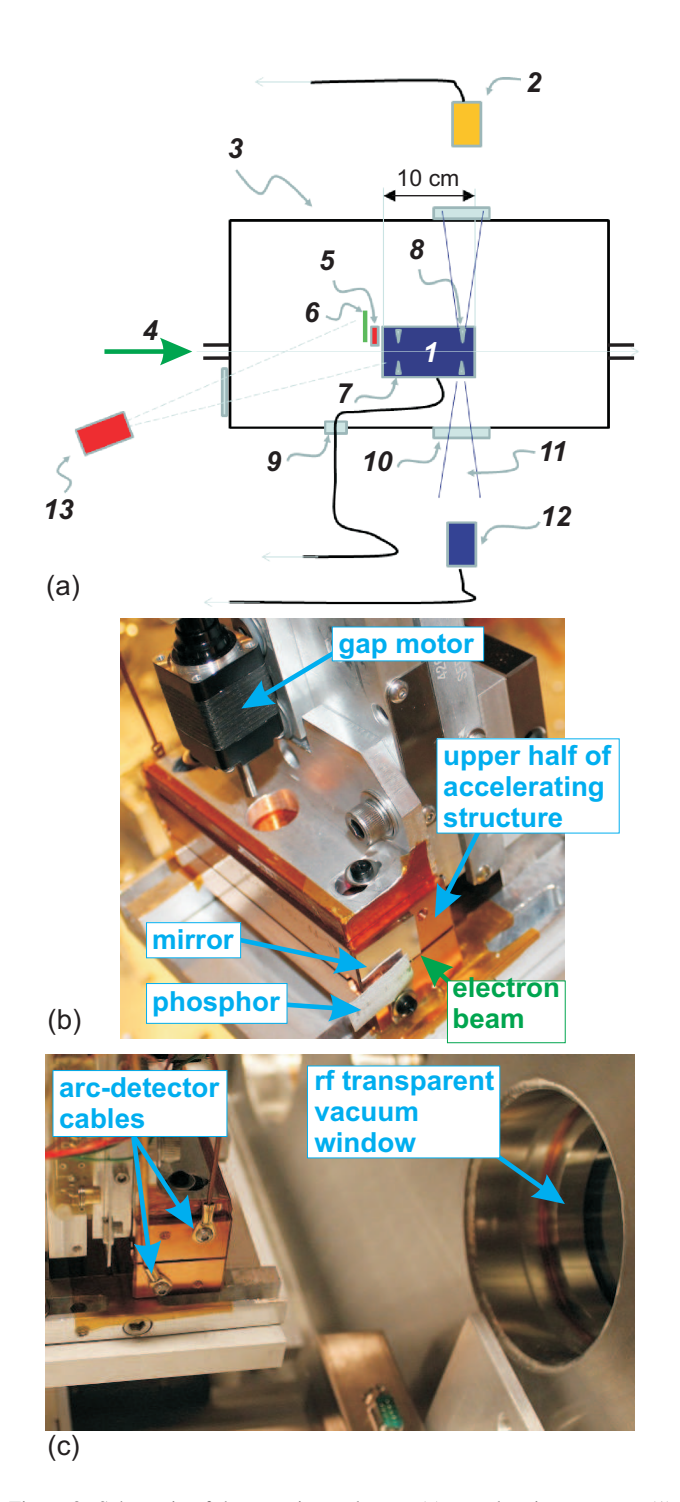


Figure 8: Schematic of the experimental setup (a): accelerating structure (1), single-shot interferometer (2), vacuum chamber (3), electron beam (4), laser alignment mirror (5), phosphor screen (6), right reflected rf horn (7), left forward rf horn (8), vacuum feed-through (9), rf window (10), output rf beam (11), interferometer (12), video camera for beam-structure alignment (13). Accelerating structure assembled on remotely controlled motorized stages (b), back side of the structure with the *arc-detector* cables connected, installed in the vacuum chamber (c).

#### 5.2. Experimental electron beam operations

During the 100 GHz copper-silver experiments, the FACET electron beam had an energy of 20.35 GeV. The experiment was performed in three shifts. In the first shift (November 21, 2015)

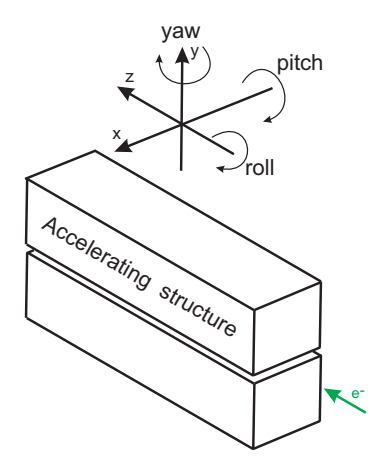


Figure 9: Definition of the three misalignment angles: yaw, pitch and roll.

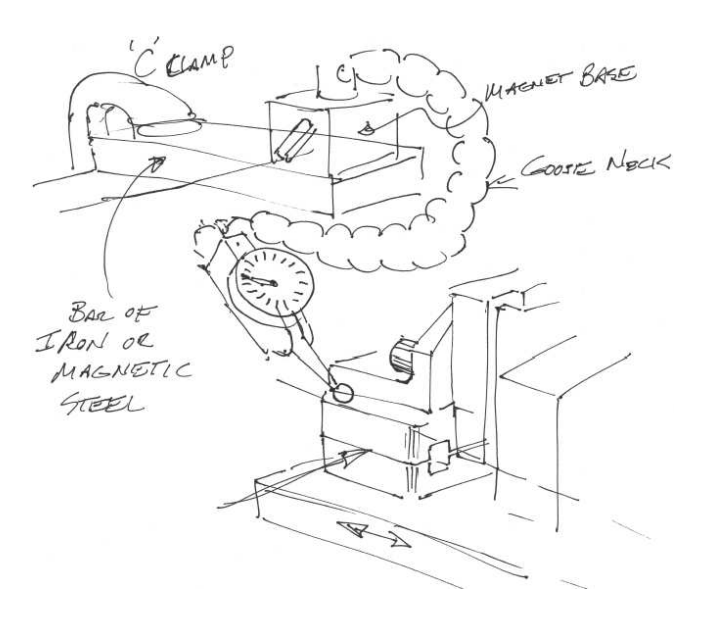


Figure 10: Original sketch of the alignment setup used to reduce the roll misalignment angle, by using the dial gauges with gooseneck. The structure is considered aligned when the gauge reading is practically constant as the structure is moved horizontally.

the bunch charge was 3.2 nC. In the second shift (November 23, 2015) the bunch charge was 2.7 nC. In the third shift (November 30, 2015) the bunch charge was 2.7 nC. The transverse (horizontal and vertical) beam size was determined by using the wire scanner, while the bunch length was determined by using a transverse deflecting cavity [28]. We summarize the bunch size measurements in Table 5.

In the second shift we measured the breakdown rate in the 100 GHz copper-silver accelerating structure. We dedicated the first and the third shifts to study the surface wave.

The common operations performed with the electron beam are the following: (i) Detect the beam on the phosphor screen: if the electron beam hits the structure, it will damage delicate parts of the corrugations. Therefore, as a first step, we must steer the beam onto the phosphor screen, which is installed far from the corrugations. (ii) Finding the vertical center of the structure: when the gap is set, we determine the vertical posi-

	$\sigma_x [\mu m]$	$\sigma_y [\mu m]$	$\sigma_z [\mu m]$
Mar 29, 2015	$45 \pm 10  \mu m$	$39 \pm 12 \mu m$	$50 \pm 8 \mu m$
	h14.55	h14.53	h3.05 (+1)
Nov 21, 2015	$25 \pm 6 \mu m$	$30 \pm 2 \mu m$	$25 \pm 2 \mu m$
	h14.18	h14.19	h14.29
Nov 23, 2015	$29 \pm 2 \mu m$	$31 \pm 4 \mu m$	$25 \pm 5 \mu m$
	h12.48	h12.54	h12.28
Nov 30, 2015	$31 \pm 2 \mu m$	$20 \pm 6 \mu m$	$25 \pm 2 \mu m$
	h17.30	h17.27	h15.28

Table 5: Summary of bunch size measurements with tolerance of the four shifts, with date and time of each measurement.

tion of the structure for which the beam is vertically centered between the two halves. This is done by setting the electron beam at an approximate vertical center (horizontally it is far from the corrugations). The structure is slowly moved up (and down), till the beam halo slightly touches the metal, generating a radiation shower, detected by photomultiplier tubes. We mark the positions of the motor where the photomultiplier voltages are approximately the same. We take the average between these two motor positions to determine vertical center of the structure. Accuracy of these measurements are determined by the shape of the transverse distribution of the beam and resolution of mover positioning. The resolution of the mover motor is about a micrometer while bunch vertical size is  $\sigma_{v}$ . Since we cannot measure the exact transverse distribution of the beam, we conjecture that the upper bound on accuracy of the location of the vertical center of the structure is  $\sigma_{v}$ . (iii) Horizontal scan: once we determined the vertical center, the structure is moved horizontally, allowing the beam to interact with the corrugations, generating electromagnetic fields. During each scan, we observed the magnitude of the energy pulses produced by the structure with pyrodetectors. (iv) The scan procedure is then repeated with different gaps. (v) Breakdown rate measurement: the beam is placed in the central axis. Breakdowns are counted using the arc-detector, while the frequency is measured with the interferometer.

We report the complete timeline of the experiments performed with the 100 GHz travelling wave accelerating structures. We followed the format established for X-band rf breakdown experiments, showing the full history of the exposure of the structure to rf fields and the corresponding behavior of the accumulated rf breakdowns. We obtained the timeline of the 100 GHz copper experiments (Mar 29, 2015 [69]) and compared it with the 100 GHz copper-silver experiments. Fig. 11(a) shows the data from the experiment with the copper accelerating structure. The beam was vertically centered between the structure halves. Fig. 11(b-c-d) shows the data from the three shifts performed with the copper-silver structure. In (b-c) we show the surface wave measurements, when the beam was offset from the vertical center and thus closer to either top or bottom half of the structure: the pyrodetector signal increases as the beam gets close to the surface. In (c) the beam was vertically centered between the structure halves. During these four shifts, we performed horizontal scans of the beam over the cavities (bell shaped curves of the pyrodetector signal), frequency measurements and collection of breakdown statistics (time intervals where the pyrodetector voltage is flat).

#### 5.3. Measurement of electron beam deflection

When the electron beam trajectory moves horizontally offaxis it excites deflecting fields, and when the beam trajectory moves far beyond the corrugations, the deflection disappears. A camera located after the vertically bending magnet records the screen image of the bunch at each pulse (see Fig. 7). The vertical screen coordinate corresponds to the beam energy. The beam optics between the test structure and the camera converts the horizontal kick angle  $\theta_x$ , generated by the structure, to a horizontal beam displacement  $\Delta x$ , given by:

$$\Delta x = R_{12} \cdot \theta_x = R_{12} \cdot \frac{eV_x}{E},$$

where  $R_{12}$  (= 14 m) is the optics coefficient that converts a beam horizontal angle into a beam horizontal displacement, given by the deflecting voltage  $V_x$  and the beam energy E. During a horizontal scan we measured the horizontal deflection of the beam centroid ( $\Delta x$ ) on the diagnostic screen, and the corresponding deflecting voltage was calculated using the electron beam optics parameter  $R_{12}$ . In this measurement, we assume that the 20 GeV beam does not receive an offset shift at the end of the structure. It only receives a change in the angle trajectory.

We simulated the transverse voltage excited by a Gaussian bunch with  $\sigma_z=25~\mu m$  and a charge of 2.7 nC (used in the 100 GHz copper-silver structure, November 23, 2015 experiment) by performing short range wakefields simulations, with GdfidL [99]. We compared the experimentally measured deflecting voltage with the simulated one. Fig. 12 shows this analysis in a horizontal scan. Vertical error bars correspond

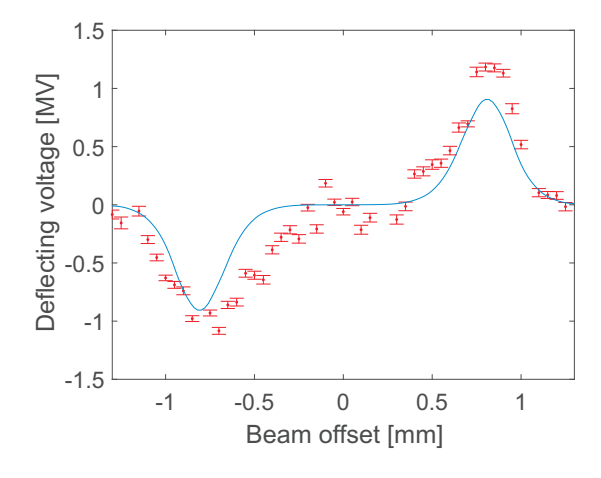


Figure 12: Measurement of beam deflection (red plot) in a horizontal scan with gap = 0.5 mm, a longitudinal bunch length  $\sigma_z = 25 \,\mu m$  and a charge of 2.7 nC (shift of November 23, 2015). Blue line is the GdfidL simulation.

to standard deviation of the centroid positions caused by transverse position jitter of the FACET bunch, pulse to pulse variation of the bunch shape and rf breakdowns. We believe that

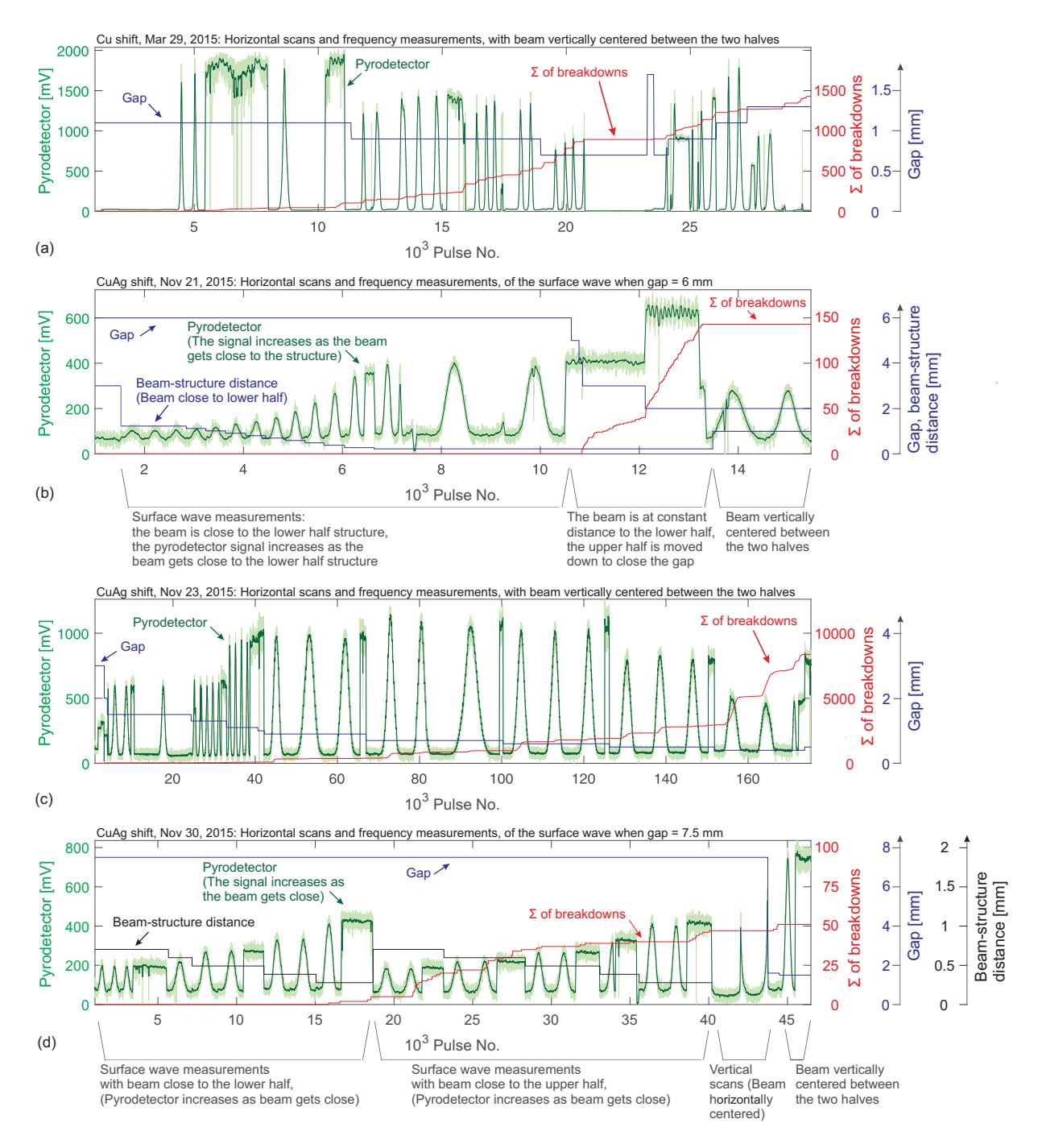


Figure 11: Timeline of the experiments performed with the 100 GHz copper accelerating structure, with 3.2 nC of bunch charge,  $\sigma_z = 50 \, \mu m$ , the gap varied from 1.7 mm to 0.7 mm (a), and timeline of the experiments performed with the 100 GHz copper-silver accelerating structure, involving the first shift with 3.2 nC of bunch charge,  $\sigma_z = 25 \, \mu m$ , the gap varied from 6 mm to 2 mm (b), second shift with 2.7 nC of bunch charge,  $\sigma_z = 25 \, \mu m$ , the gap varied from 3 mm to 0.4 mm (c), third shift with 2.7 nC of bunch charge,  $\sigma_z = 25 \, \mu m$ , the gap varied from 7.5 mm to 1.5 mm (d). The green plot is the reference pyrodetector signal, the blue is the gap, the red is the integrated number of breakdowns, recorded with the *arc-detector*. Bell shaped curves of the pyrodetector signal are generated during the horizontal scans of the beam over the cavities and flat parts are the time intervals when we performed frequency measurements and collection of breakdowns.

good correspondence between the simulated and measured deflecting voltages confirms our simulations of the accelerating voltage.

The simulation tools that we used to calculate the wake-field are confirmed by the "NOVO" code, developed by A. Novokhatski [100, 101, 102, 103]. Example of comparison between our wakefield calculations and the "NOVO" code are re-

ported in Fig. 3 of [69].

## 5.4. Measurement of breakdown rate in the copper and coppersilver structure

In this section we present the measurement and comparison of the breakdown rate, performed in the copper and in the copper-silver 100 GHz accelerating structures.

The breakdown rate measurement was performed by positioning the beam on the central axis and by exposing the structure to a certain number of pulses (flat part of the pyrodetector signal of Fig. 11. At a fixed gap, we recorded the *arc-detector* data and then calculated the corresponding breakdown rate.

These breakdown rate measurements have been performed at different gaps. The results are shown in Fig. 13, for the coppersilver structure during the second shift (Nov 23, 2016) with 2.7 nC of bunch charge and  $\sigma_z=25~\mu m$  (red plot), compared with the copper structure during the March 29, 2015 shift with 3.2 nC of bunch charge and  $\sigma_z=50~\mu m$  (blue plot). The coppersilver structure presents better breakdown rate compared with the copper structure. This result is consistent to the one obtained at X-band, where copper-silver hard alloys present better breakdown rate.

#### 5.5. Measurement of frequency with interferometer

Frequency measurements are made using a scanning Michelson Interferometer [104], shown in Fig. 8(a). A detail description of the working principle is described in [70]. The interferometer measures the autocorrelation function of the emitted signal. The Fourier transform of the autocorrelation function gives the spectral density of the signal.

Fig. 14 shows the spectrum obtained during a frequency measurement with gap = 0.9 mm. The measured frequency was 123.6 GHz.

The results of the frequency measurements as a function of the gap, performed during the 100 GHz copper-silver tests, are shown in Fig. 15, compared with the simulations. We have good agreement between simulations (blue plot) and measurements (red symbols).

## 5.6. Measurements of pulse length

We verified another prediction of the structure behavior. We determined the rf pulse length from the interferometer measurements.

For gaps larger than 3 mm, the group velocity is high, the pulse filling time is at least ten times smaller than the decay time (see Table 4). Since  $\tau_F \ll \tau_D$ , the emitted rf pulse can be approximated as truncated sine function with no damping:

$$x(t) = \begin{cases} 0 & \text{if } t \le -\tau_F, \\ A \sin(2\pi f t) & \text{if } -\tau_F < t < \tau_F, \\ 0 & \text{if } t \ge \tau_F, \end{cases}$$
 (13)

with autocorrelation function:

$$R_{x}(t) = \begin{cases} 0 & \text{if } t \le -\tau_{F}, \\ A(\tau_{F} - |t|) \cos(2\pi f t)/2 & \text{if } -\tau_{F} < t < \tau_{F}, \\ 0 & \text{if } t \ge \tau_{F}, \end{cases}$$
(14)

where A is the amplitude of the rf pulse. We fit the measured interferometer signal with the autocorrelation function, obtaining A and  $\tau_F$  as fitting parameters.

Fig. 16 show an example of fitting the measured interferometer signal, with the autocorrelation function.

The results are shown in Fig. 17. They are in good agreement with the simulations.

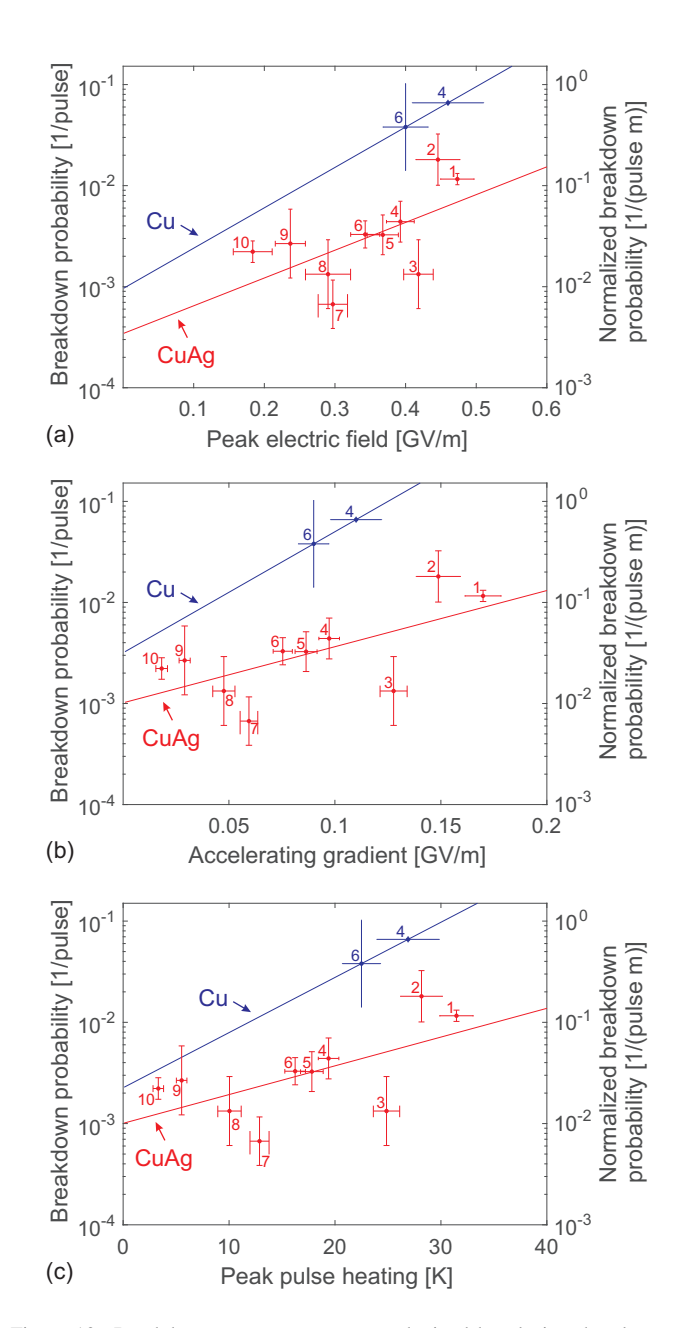


Figure 13: Breakdown rate measurements, obtained by placing the electron beam in the central axis of the structure, as a function of the peak electric field of the fundamental mode (a), as a function of the accelerating gradient (b), as a function of the peak pulsed heating (c). The red plot is the measurement performed on the copper-silver structure (second shift, Nov 23, 2016) with 2.7 nC of bunch charge and  $\sigma_z=25~\mu m$ . The blue plot is the measurement performed on the copper structure during the shift of March 29, 2015, with 3.2 nC of bunch charge and  $\sigma_z=50~\mu m$ . The number near the measurement point identifies the gap value specified in Table 4.

## 5.7. Measurements of the surface wave

The experimental measurements of the surface wave have been performed with a gap of 6 mm and 7.5 mm, which is the maximum gap allowed by our setup. With gap = 7.5 mm, gap/ $\lambda$  = 2.4 and the surface wave is still trapped between the structure halves. The picture of a structure half is shown in Fig. 18. To study the surface wave we moved one half structure

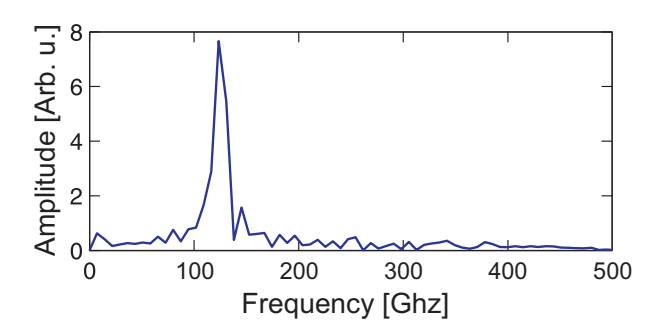


Figure 14: Spectrum of the radiated signal for gap =  $0.9~\mathrm{mm}$ . The peak frequency is 123.6 GHz

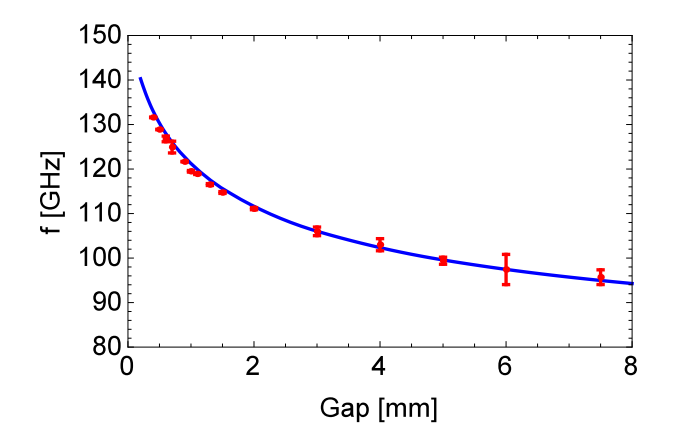


Figure 15: Plot of simulated (blue) and measured with interferometer (red) synchronous frequency of the fundamental mode as a function of the gap.

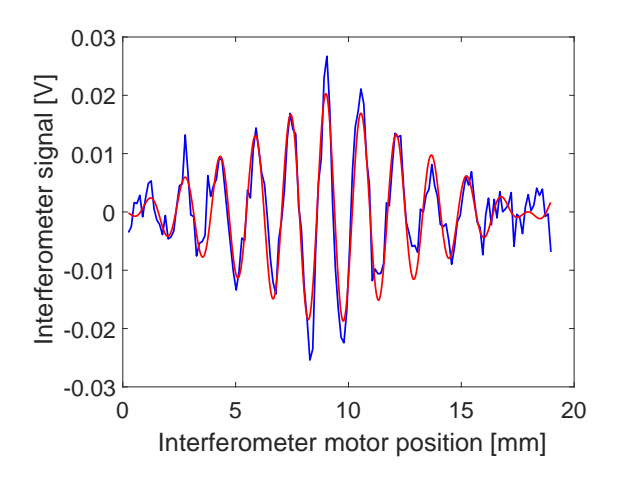


Figure 16: Measurement of the interferometer signal (blue plot) and fit of the autocorrelation function (red plot), with gap = 7.5 mm (November 30, 2015 shift). The horizontal axis is the interferometer motor position  $z_{int}$ , and it is related to the time t of Eq. 14 as:  $t = 2 \cdot (z_{int} - z_0)/c$ , where  $z_0$  is a constant.

close to the electron beam, as shown in Fig. 18.

The measurement of the surface wave properties relied on the rf radiated by the horns.

With the pyro-detector we observed that the radiated pulse energy increases when the beam trajectory gets close to the structure half (See Fig. 19). The structure couplers were designed to be matched for gap = 0.3 mm [68]. With any other

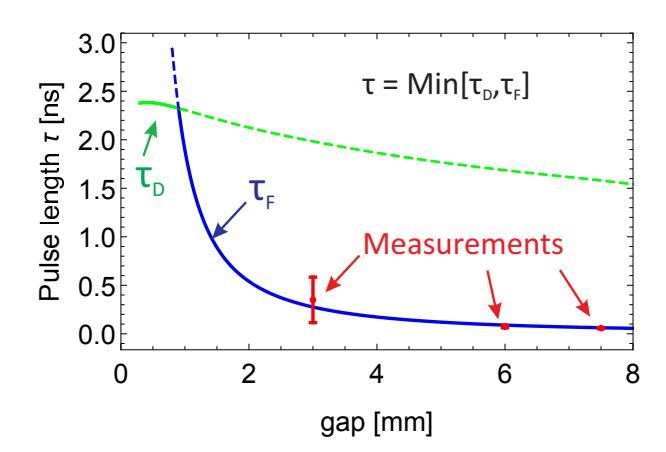


Figure 17: Plot of simulated filling time (blue), simulated decay time (green) and of the pulse length measured with interferometer (red) as a function of the gap.



Figure 18: Vertical relative position of the beam with respect to one half of the structure.

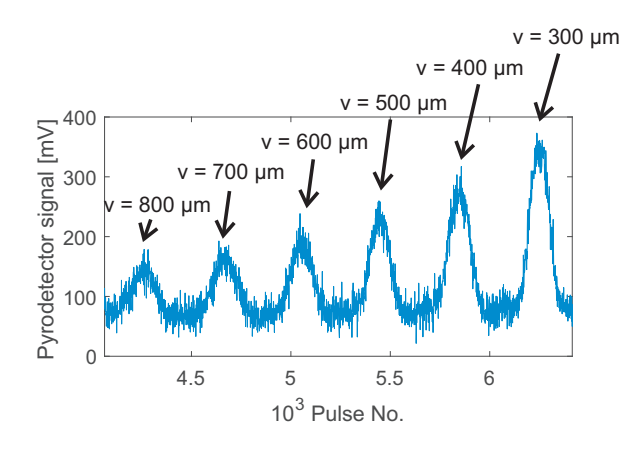


Figure 19: Pyro-detector signals, recorded during horizontal scans (bell-shaped curves), at different distances between the beam trajectory and the half structure. The measured peak energy of each horizontal scan increases when the beam gets close to the half structure. These measurements were performed at gap = 6 mm, during the November 21, 2015 shift, where the electron beam has 3.2 nC of bunch charge and  $25 \mu m$  of bunch length.

gap the coupler are mismatched but we are still able to detect the energy excited by the beam even at the maximum gap.

The measured frequencies and pulse lengths of the surface wave (when the gap is larger than 1.3 mm), are in good agreement with the simulations (see Fig. 15 and Fig. 17).

# 5.8. Scanning Electron Microscope (SEM) inspection of the copper and copper-silver structure

After the tests the accelerating structures were inspected with a scanning electron microscope. The SEM results of the experiments No. 1, 2, 5 and 6 of Table 2 (100 GHz copper structures of [68] and 200 GHz structures [70]) showed that the out-

put part of the structure is mostly damaged by rf breakdowns. These results are consistent with our understanding of breakdown behavior, because in the output part of the structure the fields are higher, the rf pulse length is the longest and thus the pulsed heating is higher. For these reasons, we were expecting to obtain similar results in our last 100 GHz tests (Experiments No. 4 and 7 of Table 2).

However the SEM inspection revealed different damage pattern in the experiment No. 4, performed with the 100 GHz copper structure (Mar 29, 2015 [69]), and in the experiment No. 7, performed with the 100 GHz copper-silver structure (Nov 21-23-30, 2015).

The results of the SEM inspection of the 100 GHz copper accelerating structure (experiment No. 4) are shown in Fig. 20. The input part of the structure shows little to no rf damage, from the input coupler to cell 54. Also the output part of the structure shows little to no rf damage, from the cell 97 to the output coupler. We found rf damage in the middle part, from cell 55 to cell 69, and from cell 81 to cell 96. With these autopsy results we conjecture that the measured breakdown rate was determined by the behavior of several cells in the middle of the structure. Possible explanations for the increase of the breakdown rate in these cells could be imperfections in the machining and in the cleaning process.

The results of the SEM inspection of the 100 GHz copper-silver accelerating structure (experiment No. 7) are shown in Fig. 21. Input and output couplers do not show obvious of rf damage. Surface melting/rf pulsed heating damage can be found on every (most) irises at high magnification. However, the damage was light compared to most previous structures of this type [68, 69, 70]. No "heavy" RF damages were found anywhere on the top and bottom blocks. This behavior is inconsistent with the first two 100 GHz experiments [68] and with the 200 GHz experiments [70], where we found the most rf damages near the output coupler, where the fields are higher and the rf pulse excited by the beam is the largest.

## 6. Discussion

In the 100 GHz experiments (No. 4 and 7 of Table 2), the breakdown behavior of copper and copper-silver was consistent with X-band, where the copper-silver structure better performed than copper. This is inconsistent with the 200 GHz experiments (No. 5 and 6 of Table 2), where the copper-silver structure performed worse than copper. We speculate that with the 200 GHz copper-silver structure the higher beam repetition rate could have increased the breakdown rate.

The SEM image pattern of the 100 GHz experiments (No. 4 and 7) is inconsistent with all other experiments where we found the most rf damages near the output coupler, where the fields are higher and the rf pulse excited by the beam is the largest, thus increasing the probability of breakdown.

The SEM autopsy of the structure used in the experiment No. 4 revealed that the input part of the structure had little to no rf damage, from the input coupler to cell 54. Also the output part of the structure had little to no rf damage, from the cell 97

to the output coupler. We found rf damage in the middle part, from cell 55 to cell 69, and from cell 81 to cell 96. We conjecture that the measured breakdown rate was determined by the behavior of several cells in the middle of the structure. Possible explanations for the increase of the breakdown rate in these cells could be imperfections in the machining and in the cleaning process. This copper structure might perform better without these imperfections.

In the 100 GHz copper-silver structure (experiments No. 7) we did not see increased damage in the output part. Possible explanations are: better structure production, better experimental conditions, better structure alignment by using the dial gauge, and lower peak pulsed surface heating (with respect the 200 GHz).

The measured breakdown rates are relatively high for the field levels and pulse lengths as compared to values extrapolated from X-band experiments [14, 9]. Typically X-band accelerating structures were conditioned by more than  $10^8$  rf pulses, without beam and vacuum pressures below  $10^{-8}$  Torr. In this experiment the rf field is excited by the FACET beam so the number of pulses was limited to  $< 10^6$  by the practical length of the experimental shift and the vacuum level is about  $10^{-6}$  Torr. We conjecture that the breakdown rate is expected to improve with a better vacuum and more conditioning time. The presence of the FACET beam could have increased the breakdown rate. The beam halo was intercepted by the structure and a few times, the whole beam was dumped into the structure due to linac faults.

#### 7. Conclusions

We report the first experimental measurements of rf breakdown statistics and frequency in a copper and copper-silver travelling-wave accelerating structure at 100 GHz frequencies. The experimental measurements of the frequency and pulse length of the radiation emitted by the structure horns are in good agreement with the calculations.

Deflecting voltage was measured by observing the displacement of the electron beam on a diagnostic screen downstream of the structure. This measurement confirms our simulated values of deflecting and accelerating gradients.

We measured the breakdown rate statistics at different gap sizes between the two structure halves, by placing the beam in the central axis. The breakdown rates measured in the 100 GHz copper and copper-silver structures are in Table 6. The copper structure has higher breakdown rate than the copper-silver one. This behavior is consistent with X-band studies, but it is inconsistent with the 200 GHz experiments results. Possible explanations for the lower breakdown rate in the 100 GHz copper-silver structure are better material properties and fewer imperfection. We conjecture that the influence of the FACET beam and the limited number of conditioning pulses both could have increased the breakdown rate. We are working on future experiments where high gradient accelerating cavities will be powered by rf sources in order to avoid the influence of the driving beam on the rf breakdown performance.

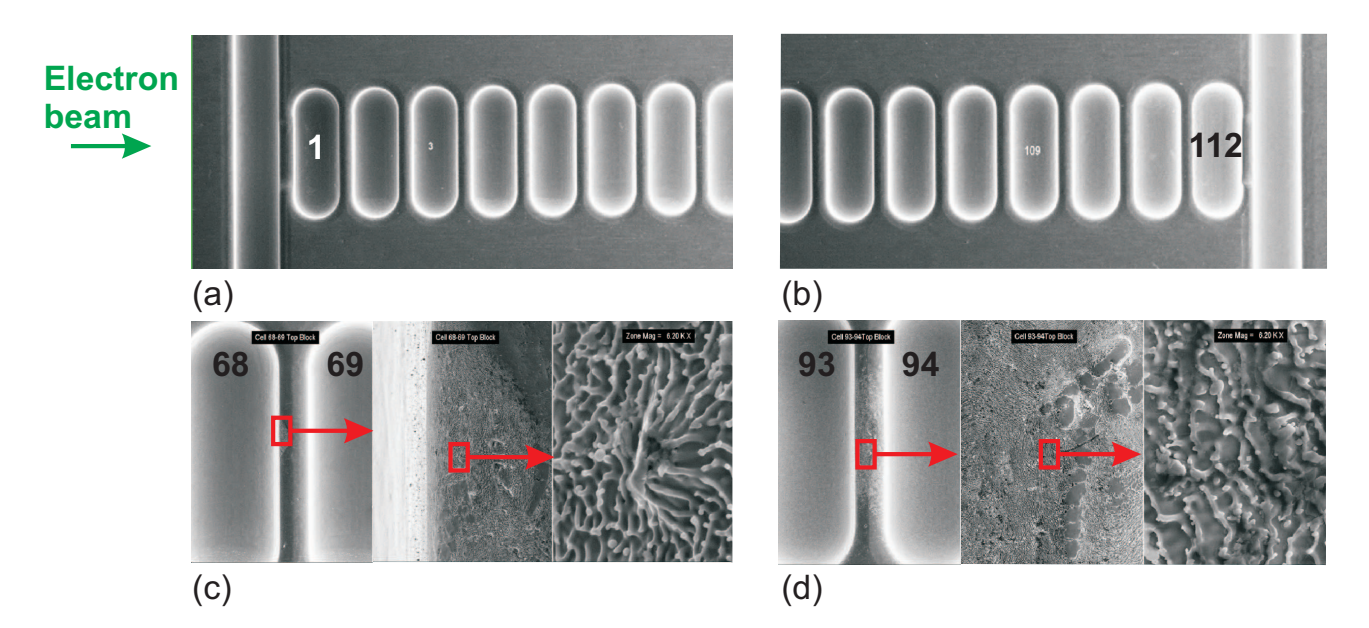


Figure 20: SEM microscope picture of the breakdown damage generated during the experiment with the 100 GHz copper structure, driven by a bunch charge of 3.2 nC and  $50 \mu m$  length. Input part of the structure: little to no damage, from the input coupler to cell 54 (a). Output end of the structure: little to no damage, from cell 97 to the output coupler (b), rf damage in the middle part of the structure, detail of the iris between cell 68 and cell 69 (c), and iris between cell 93 and cell 94 (d).

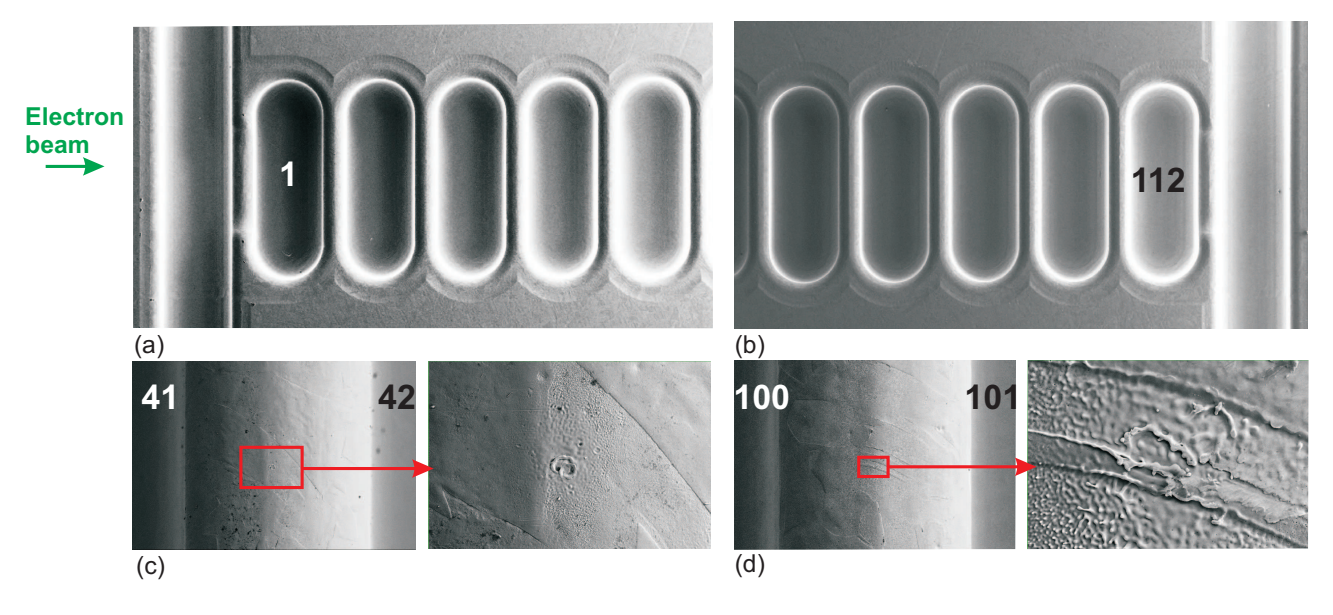


Figure 21: SEM microscope picture of the breakdown damage generated during the experiment with the 100 GHz copper-silver structure. Input (a) and output (b) couplers do not show obvious rf damage. Light surface melting/rf pulsed heating damage can be found on every (most) irises at high magnification, example in bottom cells 41-42: area of light arcing/pulsed heating (c), top cells 100-101: rf damage with widely scattered micron sized arc craters can be found (d).

We observed that a confined travelling-wave mode is trapped between the structures halves with oversized gaps, larger than the wavelength. Its behavior is consistent with the so called "surface wave". We measured the rf parameters of the surface wave, including the frequency and the pulse length, in good agreement with simulations.

These studies will pave the way towards the use of sub-THz devices in future accelerators applications.

## 8. Acknowledgments

Work supported by the US DOE under contract DE-AC02-76SF00515. We thank all the E204 experiment crew: Juan Cruz Jr., RF Diagnostics: Spencer Gessner, Oliver Williams (UCLA), Filippos Toufexis. SEM: Chris Pearson. Machine optics and other informations: Erik Adli, Carl Andreas Lindstrom, Michael Litos. We thank Vitaly Yakimenko and the FACET team for excellent support. We thank Warner Bruns for his support with the GdfidL calculation software.

Parameter	Unit	Cu	CuAg
BDR	[1/pulse]	0.066	$10^{-3}$
Norm. BDR	[1/(pulse m)]	0.66	$10^{-2}$
$E_{acc}$	[MV/m]	113	127
$E_{max(fund.mode)}$	[MV/m]	440	420
$H_{max(fund.mode)}$	[MA/m]	0.87	0.82
τ	[ns]	2.33	2.36
Pulsed heating	[K]	28	25
f	[GHz]	123	126
gap	[mm]	0.9	0.7

Table 6: Breakdown rates measured in the 100 GHz copper and copper-silver structures.

## References

- R. B. Neal (ed.), D. W. Dupen, H. A. Hogg, G. A. Loew, The Stanford two mile accelerator, W.A. Benjamin, Inc., New York, SLAC-REPRINT-1968-001, 1968.
- [2] S. Doebert, et al., High gradient performance of NLC / GLC X-band accelerating structures, in: Proc. of IEEE PAC 2005, Knoxville, Tennessee, 372–374, SLAC-PUB-11207, 2005.
- [3] J. W. Wang, R&D of accelerator structures at SLAC, High Energy Phys. Nucl. Phys. 30 (2006) 11, SLAC-PUB-12293.
- [4] G. Guignard, The CLIC Study Team, CERN Report No. CERN 2000-008, 2000
- [5] F. V. Hartemann, F. Albert, Design of a 2 MeV Compton scattering gamma-ray source for DNDO missions, in: LLNL Technical Report, LLNL-TR-416320, 2009.
- [6] D. H. Whittum, Millimeter-Wave Drivers for Future Linear Colliders, in: 22nd International Conference on Infrared and Millimeter Waves, 1998.
- [7] V. E. Balakin, O. N. Brezhnev, A. V. Novokhatsky, Yu. I. Semenov, Accelerating Structure Of A Colliding Linear Electron Positron Beam (VLEPP). Investigation Of The Maximum Attainable Acceleration Rate, SLAC-TRANS-0187, 1978.
- [8] G. A. Loew, J. W. Wang, RF Brerakdown Studies in Room Temperature Electron Linac Structures, SLAC-PUB-4647, 1988.
- [9] H. H. Braun, S. Döbert, I. Wilson, W. Wuensch, Frequency and Temperature Dependence of Electrical Breakdown at 21, 30, and 39 GHz, Phys. Rev. Lett. 90 (22) (2003) 224801, doi:10.1103/PhysRevLett.90.224801.
- [10] D. Yu, H. Henke, H. H. Braun, S. Dobert, W. Wuensch, High power test of a 30-GHz planar accelerator, in: Particle Accelerator Conference, 2001. PAC 2001. Proceedings of the 2001, vol. 5, 3858–3860 vol.5, doi: 10.1109/PAC.2001.988277, 2001.
- [11] W. W. H. Braun, M. Valentini, Test of a 30 GHz Planar Accelerating Structure in the CLIC Test Facility II, CERN-CLIC-NOTE-413.
- [12] C. Adolphsen, Normal Conducting rf Structure Test Facilities and Results, in: Proc. of IEEE PAC 2003, Portland, Oregon, 668–672, 2003.
- [13] G. Geschonke, Result form the CLIC Test Facility CTF3 and Update on the CLIC Design, in: Proceedings of EPAC08, Genoa, Italy, 2912–2916, 2008.
- [14] V. A. Dolgashev, Progress on high-gradient structures, AIP Conference Proceedings 1507 (1).
- [15] J. Wang, et al., Fabrication Technologies of the High Gradient Accelerator Structures at 100MV/M Range, in: SLAC-PUB-15146, In Proc. of IPAC10, Kyoto, Japan, 2010.
- [16] T. Higo, et al., Advances in X-band TW Acclerator Structures Operating in the 100 MV/m Regime, in: Proc. of IPAC 2010, Kyoto, Japan, 3702– 3704, 2010.
- [17] T. Higo, Progress of X-band Accelerating Structures, in: Proc. of LINAC 2010, Tsukuba, Japan, 2010.
- [18] International Workshop on Breakdown Science and High Gradient Accelerator Technology (HG2016), 2016.
- [19] N. Catalan, CERN Testing Program: Plans and Schedule, in: International Workshop on Breakdown Science and High Gradient Accelerator Technology (HG2016), 2016.
- [20] W. Wuensch, Status and objectives of the CLIC X-band activity, in: In-

- ternational Workshop on Breakdown Science and High Gradient Technology in Tsukuba, Japan, 2012.
- [21] V. Dolgashev, High gradient results from single-cell setup, in: International Workshop on Breakdown Science and High Gradient Technology in Tsukuba, Japan, 2012.
- [22] G. D'Auria, X-band technology applications at FERMI@Elettra FEL project, in: Nucl. Instr. and Meth. A(2011), 2011.
- [23] J. Beijers, et al., ZFEL: A Compact, Soft X-ray FEL in the Netherlands, in: Proc. of FEL2010, Malmo, Sweden, 163–164, 2010.
- [24] U. Amaldi, et al., Cyclinacs: Fast-Cycling Accelerators for Hadrontherapy, 2009.
- [25] A.E.Vlieks and others, Initial Testing of the Mark-0 X-Band RF Gun at SLAC, in: In Proc. IPAC 2012, New Orleans, Lousiana, USA, 2012.
- [26] P. McIntosh, et al., Realization of an X-Band RF System for LCLS, in: SLAC-PUB-11270, In Proc. of PAC05, Knoxville, Tennesee, US, 2005.
- [27] V.A. Dolgashev, X-Band Deflectors, in: Presented at ICFA Beam Dynamics Mini-Workshop on Deflecting/Crabbing Cavity Applications in Accelerators Cockcroft Institute, 1-3 September 2010, 2010.
- [28] V. A. Dolgashev, G. Bowden, Y. Ding, P. Emma, P. Krejcik, J. Lewandowski, C. Limborg, M. Litos, J. Wang, D. Xiang, Design and application of multimegawatt X-band deflectors for femtosecond electron beam diagnostics, Phys. Rev. ST Accel. Beams 17 (2014) 102801, doi:10.1103/PhysRevSTAB.17.102801.
- [29] P. Craievich, M. Petronio, S. G. Biedron, D. Castronovo, M. D. Forno, S. D. Mitri, N. Faure, D. L. Civita, G. Penco, L. Rumiz, L. Sturari, R. Vescovo, D. Wang, Implementation of Radio-Frequency Deflecting Devices for Comprehensive High-Energy Electron Beam Diagnosis, IEEE Transactions on Nuclear Science 62 (1) (2015) 210–220, ISSN 0018-9499, doi:10.1109/TNS.2014.2385155.
- [30] S.G. Tantawi and others, Application of the Balanced Hybrid Mode in Overmoded Corrugated Waveguides to Short Wavelength Dynamic Undulators, in: MOPC073, Proceedings of IPAC2011, San Sebastian, Spain, 2011.
- [31] S. Tantawi, M. Shumail, J. Neilson, G. Bowden, C. Chang, E. Hemsing, M. Dunning, Experimental Demonstration of a Tunable Microwave Undulator, Phys. Rev. Lett. 112 (2014) 164802, doi: 10.1103/PhysRevLett.112.164802.
- [32] V. Dolgashev, S. Tantawi, Y. Higashi, B. Spataro, Geometric dependence of radio-frequency breakdown in normal conducting accelerating structures, Appl. Phys. Lett. 97 (171501), doi:doi:10.1063/1.3505339.
- [33] F. Wang, C. Adolphsen, C. Nantista, Performance limiting effects in X-band accelerators, Phys. Rev. ST Accel. Beams 14 (2011) 010401, doi: 10.1103/PhysRevSTAB.14.010401.
- [34] V. A. Dolgashev, S. G. Tantawi, Simulations of Currents in X-band accelerator structures using 2D and 3D particle-in-cell code, in: Proc. of IEEE PAC 2001, Chicago, Illinois, 3807–3809, 2001.
- [35] V. Dolgashev, S. Tantawi, Effect of RF Parameters on Breakdown Limits in High-Vacuum X-Band Structures, in: AIP Conf. Proc. 691, 151, 151– 165, 2003.
- [36] V. A. Dolgashev, High magnetic fields in couplers of X-band accelerating structures, in: Proc. of IEEE PAC 2003, Portland, Oregon, 1267–1269, SLAC-PUB-10123, 2003.
- [37] V. A. Dolgashev, S. G. Tantawi, RF Breakdown in X-band Waveguides, in: Proc. of EPAC 2002, Paris, France, 2139–2141, 2002.
- [38] A. Grudiev, S. Calatroni, W. Wuensch, New local field quantity describing the high gradient limit of accelerating structures, Phys. Rev. ST Accel. Beams 12 (2009) 102001.
- [39] D. Whittum, H. Henke, P. Chou, High-gradient cavity beat-wave accelerator at W-band, in: Proceedings of PAC 1997, Vancouver, Canada, vol. 1, 542–544, doi:10.1109/PAC.1997.749753, 1997.
- [40] A. W. Chao, M. Tigner, Handbook of Accelerator Physics and Engineering, World Scientific, Singapore, 1999.
- [41] D. H. Whittum, S. G. Tantawi, Switched matrix accelerator, Review of Scientific Instruments 72 (1).
- [42] D. H. Whittum, S. G. Tantawi, Active millimeter wave accelerator with parallel beams, 1998.
- [43] SLAC W-band program.
- [44] D. Yu, S. Ben-Menahem, P. Wilson, R. Miller, R. Ruth, A. Nassiri, High frequency planar accelerating structures for future linear colliders, AIP Conference Proceedings 335 (1).
- [45] M. E. Hill, C. Adolphsen, W. Baumgartner, R. S. Callin, X. E. Lin,

- M. Seidel, T. Slaton, D. H. Whittum, High-Gradient Millimeter-Wave Accelerator on a Planar Dielectric Substrate, Phys. Rev. Lett. 87 (2001) 094801, doi:10.1103/PhysRevLett.87.094801.
- [46] M. Hill, W. Fowkes, X. Lin, D. Whittum, Beam-cavity interaction circuit at W-band, Microwave Theory and Techniques, IEEE Transactions on 49 (5) (2001) 998–1000, ISSN 0018-9480, doi:10.1109/22.920162.
- [47] M. Hill, R. Callin, M. Seidel, D. Whittum, High-power squeezetype phase shifter at W-band, Microwave Theory and Techniques, IEEE Transactions on 50 (5) (2002) 1437–1441, ISSN 0018-9480, doi: 10.1109/22.999162.
- [48] M. Hill, R. Callin, D. H. Whittum, High-power vacuum window in WR10, Microwave Theory and Techniques, IEEE Transactions on 49 (5) (2001) 994–995, ISSN 0018-9480, doi:10.1109/22.920160.
- [49] F. Zimmermann, D. H. Whittum, C. K. Ng, M. E. Hill, Wake fields in a mm-wave linac, AIP Conference Proceedings 472 (1).
- [50] H. Henke, Planar structures for electron acceleration, in: Proceedings of PAC 1995, Dallas, Texas, vol. 3, 1750–1752, doi: 10.1109/PAC.1995.505349, 1995.
- [51] B. Littmann, H. Henke, Feasibility study of optically coupling RF-power at mm waves, in: Proceedings of PAC 1995, vol. 3, 1593–1595, doi: 10.1109/PAC.1995.505297, 1995.
- [52] W. Bruns, Design of input couplers and endcells for side coupled muffintin structures, in: Proceedings of PAC 1995, Dallas, Texas, vol. 2, 1088– 1089, doi:10.1109/PAC.1995.505138, 1995.
- [53] W. Bruns, Error sensitivity study for side coupled muffin tin structures using a finite difference program, in: Proceedings of PAC 1995, Dallas, Texas, vol. 2, 1085–1087, doi:10.1109/PAC.1995.505137, 1995.
- [54] P. Chou, G. Bowden, M. Copeland, H. Henke, A. Menegat, R. Siemann, Design and fabrication of a traveling-wave muffin-tin accelerating structure at 90 GHz, in: Proceedings of PAC 1997, vol. 1, 464–466, doi: 10.1109/PAC.1997.749688, 1997.
- [55] P. J. Chou, G. B. Bowden, M. R. Copeland, A. Farvid, R. E. Kirby, A. Menegat, C. Pearson, L. Shere, R. H. Siemann, J. E. Spencer, D. H. Whittum, The fabrication of millimeter-wavelength accelerating structures, AIP Conference Proceedings 398 (1).
- [56] P. Chou, G. Bowden, M. Copeland, H. Henke, A. Menegat, D. Pritzkau, R. Siemann, RF measurements of a traveling wave muffin-tin accelerating structure at 90 GHz, in: Proceedings of PAC 1997, vol. 1, 672–674, doi:10.1109/PAC.1997.749801, 1997.
- [57] N. Kroll, E. Hill, X. Lin, R. Siemann, D. Vier, D. Whittum, D. Palmer, Planar accelerator structures for millimeter wavelengths, in: Proceedings of PAC 1999, vol. 5, 3612–3614, doi:10.1109/PAC.1999.792387, 1999
- [58] Facility for Advanced Accelerator Experimental Tests, FACET.
- [59] B. D. O'Shea, G. Andonian, S. K. Barber, K. L. Fitzmorris, S. Hakimi, J. Harrison, P. D. Hoang, M. J. Hogan, B. Naranjo, O. B. Williams, V. Yakimenko, J. B. Rosenzweig, Observation of acceleration and deceleration in gigaelectron-volt-per-metre gradient dielectric wakefield accelerators, Nature Communications 7 (2016) 12763 EP -, URL http://dx.doi.org/10.1038/ncomms12763, article.
- [60] G. Andonian, D. Stratakis, M. Babzien, S. Barber, M. Fedurin, E. Hemsing, K. Kusche, P. Muggli, B. O'Shea, X. Wei, O. Williams, V. Yakimenko, J. B. Rosenzweig, Dielectric Wakefield Acceleration of a Relativistic Electron Beam in a Slab-Symmetric Dielectric Lined Waveguide, Phys. Rev. Lett. 108 (2012) 244801, doi: 10.1103/PhysRevLett.108.244801.
- [61] M. C. Thompson, H. Badakov, J. B. Rosenzweig, G. Travish, M. Hogan, R. Ischebeck, N. Kirby, R. Siemann, D. Walz, P. Muggli, et al., Ultra-High Gradient Dielectric Wakefield Accelerator Experiments, URL http://www.osti.gov/scitech/servlets/purl/894768, 2006.
- [62] M. C. Thompson, H. Badakov, A. M. Cook, J. B. Rosenzweig, R. Tikhoplav, G. Travish, I. Blumenfeld, M. J. Hogan, R. Ischebeck, N. Kirby, R. Siemann, D. Walz, P. Muggli, A. Scott, R. B. Yoder, Breakdown Limits on Gigavolt-per-Meter Electron-Beam-Driven Wakefields in Dielectric Structures, Phys. Rev. Lett. 100 (2008) 214801, doi: 10.1103/PhysRevLett.100.214801.
- [63] J. B. Rosenzweig, G. Andonian, P. Muggli, P. Niknejadi, G. Travish, O. Williams, K. Xuan, V. Yakimenko, High Frequency, High Gradient Dielectric Wakefield Acceleration Experiments at SLAC and BNL, AIP Conference Proceedings 1299 (1).
- [64] D. Wang, S. Antipov, C. Jing, J. G. Power, M. Conde, E. Wisniewski,

- W. Liu, J. Qiu, G. Ha, V. Dolgashev, C. Tang, W. Gai, Interaction of an Ultrarelativistic Electron Bunch Train with a W-Band Accelerating Structure: High Power and High Gradient, Phys. Rev. Lett. 116 (2016) 054801, doi:10.1103/PhysRevLett.116.054801, URL http://link.aps.org/doi/10.1103/PhysRevLett.116.054801.
- [65] W. Gai, P. Schoessow, B. Cole, R. Konecny, J. Norem, J. Rosenzweig, J. Simpson, Experimental Demonstration of Wake-Field Effects in Dielectric Structures, Phys. Rev. Lett. 61 (1988) 2756–2758, doi:10.1103/PhysRevLett.61.2756, URL http://link.aps.org/doi/10.1103/PhysRevLett.61.2756.
- [66] M. Conde, S. Antipov, W. Gai, C. Jing, R. Konecny, W. Liu, J. Power, H. Wang, Z. Yusof, The Argonne Wakefield Accelerator Facility: Status and Recent Activities, in: Particle Accelerator Conference, 2005. PAC 2005. Proceedings of the, 1485–1487, doi:10.1109/PAC.2005.1590808, 2005
- [67] M. Conde, Survey of advanced dielectric wakefield accelerators, in: Particle Accelerator Conference, 2007. PAC. IEEE, 1899–1903, doi: 10.1109/PAC.2007.4441323, 2007.
- [68] M. Dal Forno, V. Dolgashev, G. Bowden, C. Clarke, M. Hogan, D. McCormick, A. Novokhatski, B. Spataro, S. Weathersby, S. G. Tantawi, rf breakdown tests of mm-wave metallic accelerating structures, Phys. Rev. Accel. Beams 19 (2016) 011301, doi: 10.1103/PhysRevAccelBeams.19.011301.
- [69] M. Dal Forno, V. Dolgashev, G. Bowden, C. Clarke, M. Hogan, D. Mc-Cormick, A. Novokhatski, B. Spataro, S. Weathersby, S. G. Tantawi, Experimental measurements of rf breakdowns and deflecting gradients in mm-wave metallic accelerating structures, Phys. Rev. Accel. Beams 19 (2016) 051302, doi:10.1103/PhysRevAccelBeams.19.051302, URL http://link.aps.org/doi/10.1103/PhysRevAccelBeams.19.051302.
- [70] M. Dal Forno, V. Dolgashev, G. Bowden, C. Clarke, M. Hogan, D. McCormick, A. Novokhatski, B. O'Shea, B. Spataro, S. Weathersby, S. G. Tantawi, rf breakdown measurements in electron beam driven 200 GHz copper and copper-silver accelerating structures, Phys. Rev. Accel. Beams 19 (2016) 111301, doi:10.1103/PhysRevAccelBeams.19.111301, URL http://link.aps.org/doi/10.1103/PhysRevAccelBeams.19.111301.
- [71] High Frequency Structural Simulator, HFSS.
- [72] A. Smirnov, Group velocity effect on resonant, long-range wake-fields in slow wave structures, Nucl. Instr. and Meth. A 480 (2-3) (2002) 387 – 397, ISSN 0168-9002, doi:http://dx.doi.org/10.1016/S0168-9002(01)01233-5.
- [73] K. L. F. Bane, G. Stupakov, Impedance of a rectangular beam tube with small corrugations, Phys. Rev. ST Accel. Beams 6 (2003) 024401, doi: 10.1103/PhysRevSTAB.6.024401.
- [74] A. Millich, L. Thorndahl, Loss factor dependence on group velocity in disk-loaded travelling-wave structures, CERN-CLIC-NOTE-366.
- [75] C. Nantista, S. Tantawi, V. A. Dolgashev, Low-field accelerator structure couplers and design techniques, Phys. Rev. ST Accel. Beams 7 (2004) 072001, 7 pages.
- [76] M. Dal Forno, P. Craievich, G. Penco, R. Vescovo, Theoretical and experimental analysis of a linear accelerator endowed with single feed coupler with movable short-circuit, Review of Scientific Instruments 84 (11) 114701
- [77] P. B. Wilson, Scaling linear colliders to 5 TeV and above, AIP Conference Proceedings 397 (1).
- [78] L. Laurent, S. Tantawi, V. Dolgashev, C. Nantista, Y. Higashi, M. Aicheler, S. Heikkinen, W. Wuensch, Experimental study of rf pulsed heating, Phys. Rev. ST Accel. Beams 14 (041001), doi: 10.1103/PhysRevSTAB.14.041001.
- [79] D. P. Pritzkau, R. H. Siemann, Experimental study of rf pulsed heating on oxygen free electronic copper, Phys. Rev. ST Accel. Beams 5 (11) (2002) 112002, doi:10.1103/PhysRevSTAB.5.112002.
- [80] V. Dolgashev, S. Tantawi, Y. Higashi, T. Higo, Status of High Power Tests of Normal Conducting Single-cell Structures, in: Proc. of EPAC 2008, Genoa, Italy, 742–744, 2008.
- [81] C. C. Cutler, Genesis of the corrugated electromagnetic surface, in: Antennas and Propagation Society International Symposium, 1994. AP-S. Digest, vol. 3, 1456–1459 vol.3, doi:10.1109/APS.1994.408225, 1994.
- [82] G. Goubau, Single-Conductor Surface-Wave Transmission Lines, Proceedings of the IRE 39 (6) (1951) 619–624, ISSN 0096-8390, doi: 10.1109/JRPROC.1951.233782.

- [83] G. Goubau, On the Excitation of Surface Waves, Proceedings of the IRE 40 (7) (1952) 865–868, ISSN 0096-8390, doi: 10.1109/JRPROC.1952.273856.
- [84] G. Goubau, Open Wire Lines, IRE Transactions on Microwave Theory and Techniques 4 (4) (1956) 197–200, ISSN 0097-2002, doi: 10.1109/TMTT.1956.1125062.
- [85] W. Rotman, A Study of Single-Surface Corrugated Guides, Proceedings of the IRE 39 (8) (1951) 952–959, ISSN 0096-8390, doi: 10.1109/JRPROC.1951.273719.
- [86] Electromagnetic surface waveguides, a review, India, IEE-IERE Proceedings - 15 (4) (1977) 139–171, ISSN 0018-9146, doi: 10.1049/iipi.1977.0043.
- [87] H. M. Barlow, Surface Waves, Proceedings of the IRE 46 (7) (1958) 1413–1417, ISSN 0096-8390, doi:10.1109/JRPROC.1958.287016.
- [88] S. J. Smith, E. M. Purcell, Visible Light from Localized Surface Charges Moving across a Grating, Phys. Rev. 92 (1953) 1069–1069, doi:10.1103/PhysRev.92.1069, URL http://link.aps.org/doi/10.1103/PhysRev.92.1069.
- [89] J. H. Booske, R. J. Dobbs, C. D. Joye, C. L. Kory, G. R. Neil, G. S. Park, J. Park, R. J. Temkin, Vacuum Electronic High Power Terahertz Sources, IEEE Transactions on Terahertz Science and Technology 1 (1) (2011) 54–75, ISSN 2156-342X, doi:10.1109/TTHZ.2011.2151610.
- [90] P. Emma, M. Venturini, K. L. F. Bane, G. Stupakov, H.-S. Kang, M. S. Chae, J. Hong, C.-K. Min, H. Yang, T. Ha, W. W. Lee, C. D. Park, S. J. Park, I. S. Ko, Experimental Demonstration of Energy-Chirp Control in Relativistic Electron Bunches Using a Corrugated Pipe, Phys. Rev. Lett. 112 (2014) 034801, doi:10.1103/PhysRevLett.112.034801, URL http://link.aps.org/doi/10.1103/PhysRevLett.112.034801.
- [91] M. Guetg, et al., Commissioning of the RadiaBeam / SLAC Dechirper, in: Proceedings, 7th International Particle Accelerator Conference (IPAC 2016): Busan, Korea, May 8-13, 2016, MOPOW044, doi:10.18429/JACoW-IPAC2016-MOPOW044, URL http://inspirehep.net/record/1469736/files/mopow044.pdf, 2016
- [92] S. Bettoni, P. Craievich, A. A. Lutman, M. Pedrozzi, Temporal profile measurements of relativistic electron bunch based on wakefield generation, Phys. Rev. Accel. Beams 19 (2016) 021304, doi:10.1103/PhysRevAccelBeams.19.021304, http://link.aps.org/doi/10.1103/PhysRevAccelBeams.19.021304.
- [93] A. Novokhatski, et al., RadiaBeam/SLAC Dechirper as a Passive Deflector, in: Proceedings, 7th International Particle Accelerator Conference (IPAC 2016): Busan, Korea, May 8-13, 2016, MOPOW046, doi:10.18429/JACoW-IPAC2016-MOPOW046, URL http://inspirehep.net/record/1469738/files/mopow046.pdf, 2016
- [94] V. Dolgashev, Attosecond Diagnostics of Multi-GeV Electron Beams Using W-Band Deflectors, URL http://www.feis-2.org, proceeding of FEIS-2: Femtosecond Electron Imaging and Spectroscopy, East Lansing, Michigan, 2015.
- [95] A. Novokhatski, Wakefield potentials of corrugated structures, Phys. Rev. ST Accel. Beams 18 (2015) 104402, doi:10.1103/PhysRevSTAB.18.104402, URL http://link.aps.org/doi/10.1103/PhysRevSTAB.18.104402.
- [96] EDM Department Inc., Bartlett, IL, USA.
- [97] J. Wang, J. Lewandowski, J. Van Pelt, C. Yoneda, B. Gudkov, G. Riddone, T. Higo, T. Takatomi, Fabrication Technologies of the High Gradient Accelerator Structures at 100MV/m Range, Conf. Proc. C100523 (2010) THPEA064.
- [98] J. Wang, Surface Treatment Issues for RF Structure Fabrication, in: X-band Accelerating Structure Review, 2014.
- [99] GdfidL, Germany.
- [100] A. Novokhatsky, The Computer Code NOVO for the Calculation of Wake Potentials of the Very Short Ultra-relativistic Bunches, SLAC-PUB-11556, 2005.
- [101] A. Novokhatski, Field dynamics of coherent synchrotron radiation using a direct numerical solution of Maxwell's equations, Phys. Rev. ST Accel. Beams 14 (2011) 060707, doi:10.1103/PhysRevSTAB.14.060707.
- [102] A. Novokhatsky, Modeling of Coherent Synchrotron Radiation using a Direct Numerical Solution of Maxwell's Equations, SLAC-PUB-15258, 2012.
- [103] V. Balakin, I. Koop, A. Novokhatski, A. S. Skrinski, V. Smirnov, Beam

- Dynamics Of A Colliding Linear Electron Positron Beam (VLEPP), SLAC-TRANS-0188, 1978.
- [104] A. A. Michelson, E. W. Morley, On the Relative Motion of the Earth and of the Luminiferous Ether, Sidereal Messenger, vol. 6, pp.306-310 6 (1887) 306-310.